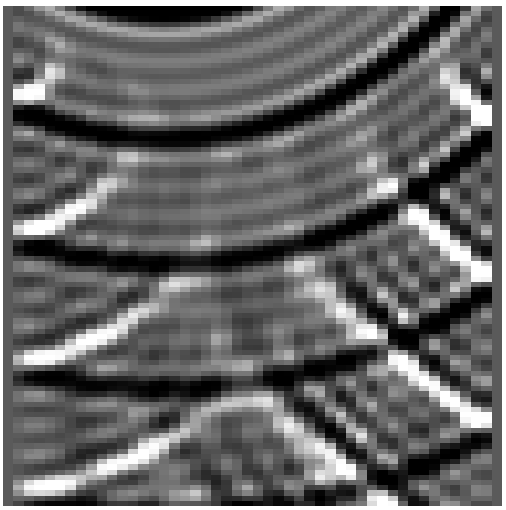

Figure 4.7: Modify the program so that zero-slope side boundaries are replaced by zero-value side boundaries. omx-Mzeroslope [ER]

The zero slope boundary condition is explicitly visible as identical signal on the two end columns. Likewise, the zero-value side boundary condition has a column of zero-valued signal on each side. In each case, the end trace need not be explicitly present, and it is not present in Dave Hale's coding of the boundary conditions which I give, but do not derive, below.

```
p0 = bl * p(1);          pnxp1 = br * p(nx)

cd(1)   =  aa * p(2)    + ( 1. - 2. * aa ) * p( 1) + aa * p0
cd(nx)  =  aa * p(nx-1) + ( 1. - 2. * aa ) * p(nx) + aa * pnxp1

endl  =  c * bl + b;
endr  =  a * br + b

call ctris(nx,endl,a,b,c,endr,cd,p,ce,cf)
```

Note that `bl=br=0` for zero-value boundaries, and `bl=br=1` for zero-slope boundaries. Absorbing side boundaries, derived in chapter 9 are obtained by letting `bl` and `br` be complex.

4.3.5 Including lateral velocity variation

Lateral velocity variation $v = v(x)$ has not been included in the program, but it is not difficult to install. It enters in two places. It enters first in equation (4.60). If the wavefield is such that k_x is small enough, then equation (4.60) is the only place it is needed. Second, it enters in the tridiagonal coefficients through the v in equation (4.56). The so-called thin-lens approximation of optics seems to amount to including the equation (4.60) part only. An example of lateral velocity variation is in Figure 4.8.

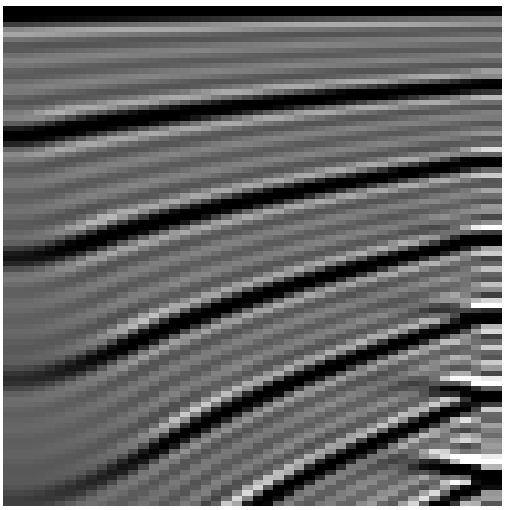

Figure 4.8: Make changes to the program to include a thin-lens term with a lateral velocity change of 40% across the frame produced by a constant slowness gradient. Identify other parts of the program which are affected by lateral velocity variation. You need not make these other changes. Why are they expected to be small? omx-Mlateralvel [ER]

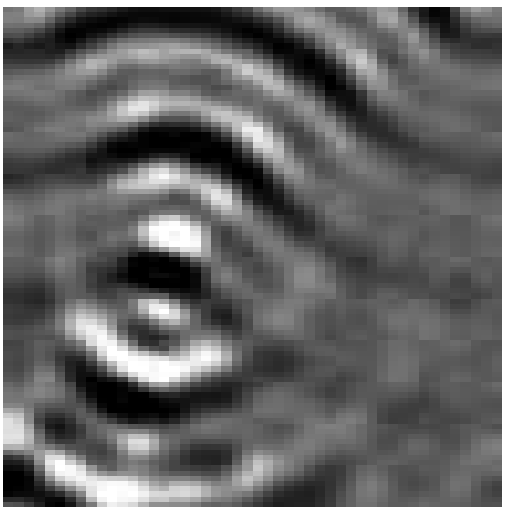

Figure 4.9: Incorporate the 45° term, ∂_{xxz}, for the collapsing spherical wave. Use zero-slope sides. Compare your result with the 15° result obtained via the program `wavemovie`. Mark an X at the theoretical focus location. omx-Mfortyfive [ER]

4.3.6 Phase shift

Theory predicts that in two dimensions, waves going through a focus suffer a 90° phase shift. You should be able to notice that a symmetrical waveform is incident on the focus, but an antisymmetrical waveform emerges. This is easily seen in Figure 4.10.

In migrations, waves go just *to* a focus, not *through* it. So the migration impulse

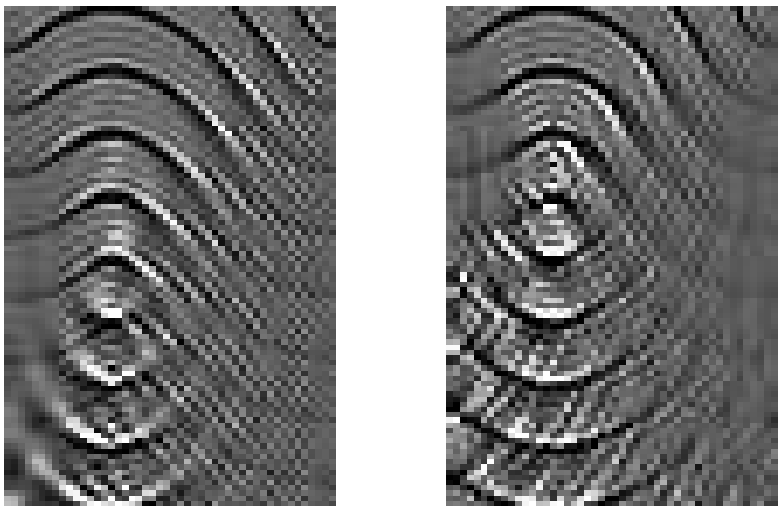

Figure 4.10: The accuracy of the x-derivative may be improved by a technique that is analyzed later in chapter 8. Briefly, instead of representing $k_x^2 \Delta x^2$ by the tridiagonal matrix $\mathbf{T}$ with $(-1, 2, -1)$ on the main diagonal, you use $\mathbf{T}/(\mathbf{I} - \mathbf{T}/6)$. Modify the extrapolation analysis by multiplying through by the denominator. Make the necessary changes to the 45° collapsing wave program. Left without 1/6 trick; right, with 1/6 trick. omx-trick [ER]

response in two dimensions carries a 45° phase shift. Even though real life is three dimensional, the two-dimensional response is appropriate for migrating seismic lines where focusing is presumed to arise from cylindrical, not spherical, reflectors.

4.4 MIGRATION IN THE (omega,x)-DOMAIN (KJ)

The migration program is similar to the film loop program. But there are some differences. The film loop program has "do loops" nested four deep. It produces results for many values of t. Migration requires a value only at $t = 0$. So one loop is saved, which means that for the same amount of computer time, the space volume can be increased. Unfortunately, loss of a loop seems also to mean loss of a movie. With ω-domain migration, it seems that the only interesting thing to view is the input and the output.

The input for this process will probably be field data, unlike for the film loop movie, so there will not be an analytic representation in the ω-domain. The input will be in the time domain and will have to be Fourier transformed. The beginning of the program defines some pulses to simulate field data. The pulses are broadened

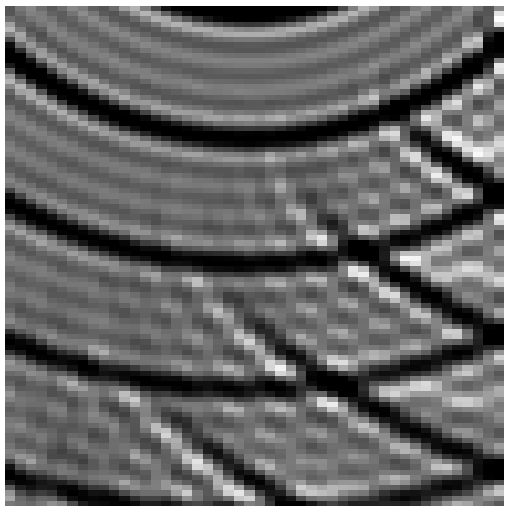

Figure 4.11: Chapter 9 explains how to absorb energy at the side boundaries. Make the necessary changes to the program to absorb waves incident on the left-side boundary. omx-Mabsorbside [ER]

impulses and should migrate to approximate semicircles. Exact impulses were not used because the departure of difference operators from differential operators would make a noisy mess.

Next the program Fourier transforms the pseudodata from the time domain into the ω-frequency domain.

Then comes the downward continuation of each frequency. This is a loop on depth z and on frequency ω. Either of these loops may be on the inside. The choice can be made for machine-dependent efficiency.

For migration an equation for upcoming waves is required, unlike the downgoing wave equation required for the film loop program. Change the sign of the z-axis in equation (4.53). This affects the sign of `aa` and the sign of the phase of `cshift`.

Another difference with the film loop program is that the input now has a time axis whereas the output is still a depth axis. It is customary and convenient to reorganize the calculation to plot travel-time depth, instead of depth, making the vertical axes on both input and output the same. Using $\tau = z/v$, equivalently $d\tau/dz = 1/v$, the chain rule gives

$$\frac{\partial}{\partial z} = \frac{\partial \tau}{\partial z}\,\frac{\partial}{\partial \tau} = \frac{1}{v}\,\frac{\partial}{\partial \tau} \tag{4.61}$$

Substitution into (4.53) gives

$$\frac{\partial P}{\partial \tau} = -i\,\omega\,P - \frac{v^2}{-i\,\omega\,2}\,\frac{\partial^2 P}{\partial x^2} \tag{4.62}$$

In the program, the time sample size `dt` $= \Delta t$ and the travel-time depth sample `dtau` $= \Delta\tau$ are taken to be unity, so the maximum frequency is the Nyquist. Notice that the frequency loop covers only the positive frequency axis. The negative frequencies serve only to keep the time function real, a task that is more easily done by simply taking the real part. A program accompanies.

```
#%  Migration in the (omega,x,z)-domain
subroutine kjartjac()
real p(48,64), pi, alpha, dt, dtau, dw, w0, omega
complex cp(48,64), cd(48), ce(48), cf(48), aa, a, b, c, cshift
integer ix, nx, iz, nz, iw, nw, it, nt, esize
nt= 64;   nz= nt;    nx= 48;      pi= 3.141592
dt= 1.;   dtau= 1.;  w0=-pi/dt;   dw= 2*pi/(dt*nt);    nw= nt/2;
alpha = .25                                  #  alpha = v*v*dtau/(4*dx*dx)
do iz= 1, nz { do ix=1,nx { p(ix,iz) = 0.;    cp(ix,iz)=0. }}
do it= nt/3, nt, nt/4
        do ix= 1, 4                          # Broadened impulse source
                { cp(ix,it) = (5.-ix);     cp(ix,it+1) = (5.-ix) }
call ft2axis( 0, 1., nx,nt, cp)
do iz= 1, nz {
do iw= 2, nw {    omega = w0 + dw*(iw-1)
        aa = - alpha /( (0.,-1.)*omega )
        a = -aa;      b = 1.+2.*aa;      c = -aa
        do ix= 2, nx-1
                cd(ix) = aa*cp(ix+1,iw) + (1.-2.*aa)*cp(ix,iw) + aa*cp(ix-1,iw)
        cd(1) = 0.;      cd(nx) = 0.
        call ctris( nx, -a, a, b, c, -c, cd, cp(1,iw))
        cshift = cexp( cmplx( 0.,-omega*dtau))
        do ix= 1, nx
                cp(ix,iw) = cp(ix,iw) * cshift
        do ix= 1, nx
                p(ix,iz) = p(ix,iz)+cp(ix,iw)   # p(t=0) = Sum P(omega)
        }}
esize=4
to history:     integer n1:nx, n2:nz, esize
call hclose()
call srite( 'out', p, nx*nz*4 )
return; end
```

The output of the program is shown in Figure 4.12. Mainly, you see semicircle approximations. There are also some artifacts at late time that may be ω-domain wraparounds. The input pulses were apparently sufficiently broad-banded in dip that the figure provides a preview of the fact, to be proved later, that the actual semicircle approximation is an ellipse going through the origin.

Notice that the waveform of the original pulses was a symmetric function of time, whereas the semicircles exhibit a waveform that is neither symmetric nor antisymmetric, but is a 45° phase-shifted pulse. Waves from a point in a three-dimensional world would have a phase shift of 90°. Waves from a two-dimensional exploding reflector in a three-dimensional world have the 45° phase shift.

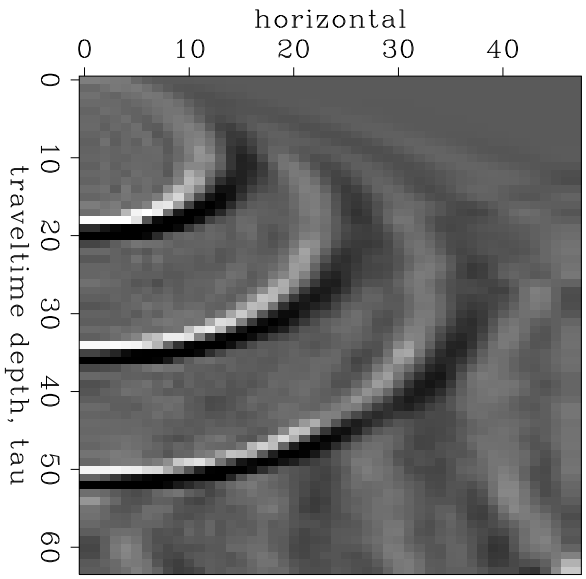

Figure 4.12: Output of the program `kjartjac`: semicircle approximations. omx-kjartjac [ER]

Chapter 5

Splitting and working in the time domain

Here we will first look at some general principles having to do with splitting a process into separate, but simpler processes, and how this can be understood by inspecting differential equations. Then we'll look at finite-difference migration in the time domain.

Figure 5.1 illustrates the differences between Fourier domain calculations and time domain calculations. The figure was calculated on a 256×64 mesh to exacerbate for

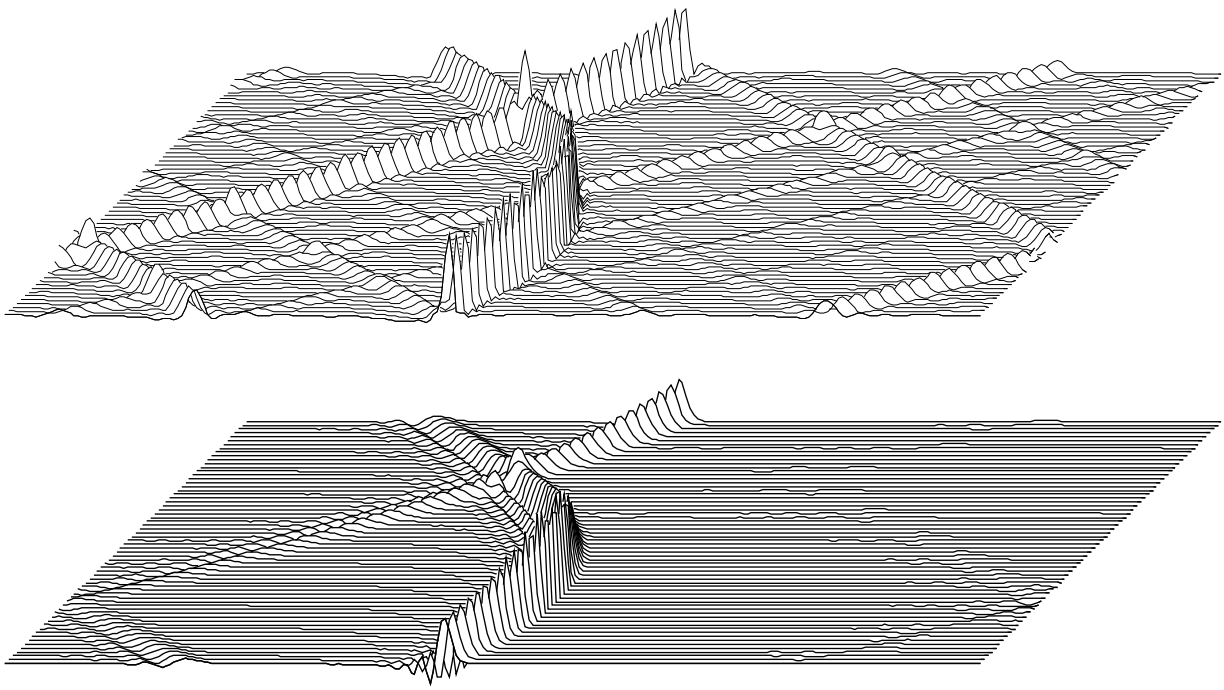

Figure 5.1: Frequency domain hyperbola (top) and time domain hyperbola (bottom). txz-freqhyp [NR]

display the difficulties in either domain. Generally, you notice wraparound noise in the

Fourier calculation, and frequency dispersion in the time domain calculation. (The "time domain" hyperbola in Figure 5.1 is actually a frequency domain simulation—to wrap the entire hyperbola into view). In this chapter we will see how to do the time domain calculations. A more detailed comparison of the domains is in chapter 8.

Even if you always migrate in the frequency domain, it is worth studying time domain methods to help you choose parameters to get a good time domain response. For example both parts of Figure 5.1 were done in the frequency domain, but one simulated the time domain calculation to get a more causal response.

Much of seismology amounts to measuring time shifts. The word *stepout* denotes a change of travel time with a change in location. Frequency-domain calculations usually conclude with a transform to the time domain to let us see the shifts. An advantage of time-domain computations is that time shifts of wave packets can be measured as the computation proceeds. In the frequency domain it is not difficult to reference one single time point, or to prescribe a shift of the whole time function. But it is not easy to access separate wavelets or wave packets without returning to the time domain.

The upward and downward wavefield extrapolation filter $\exp[i\, k_z(\omega, k_x)z]$ is basically a causal all-pass filter. (Under some circumstances it is anticausal). It moves energy around without amplification or attenuation. I suppose this is why migration filtering is more fun than minimum-phase filtering. Migration filters gather energy from all over and drop it in a good place, whereas minimum-phase filters hardly move things at all—they just scale some frequencies up and others down.

5.1 SPLITTING AND FULL SEPARATION

Two processes, **A** and **B**, which ordinarily act simultaneously, may or may not be interconnected. The case where they are independent is called *full separation.* In this case it is often useful, for thought and for computation, to imagine process **A** going to completion before process **B** is begun. Where the processes are interconnected it is possible to allow **A** to run for a short while, then switch to **B**, and continue in alternation. This alternation approach is called *splitting.*

5.1.1 The heat-flow equation

The diffraction or migration equation could be called the "wavefront healing" equation. It smooths back together any lateral breaks in the wavefront that may have been caused by initial conditions or by the lens term. The 15° migration equation has the same mathematical form as the heat-flow equation. But the heat-flow equation has all real numbers, and its physical behavior is more comprehensible. This makes it a worthwhile detour. A two-sentence derivation of it follows. (1) The heat flow H_x in the x-direction equals the negative of the gradient $-\partial/\partial x$ of temperature T times the heat conductivity σ. (2) The decrease of temperature $-\partial T/\partial t$ is proportional to

the divergence of the heat flow $\partial H_x/\partial x$ divided by the heat storage capacity C of the material. Combining these, extending from one dimension to two, taking σ constant and $C = 1$, gives the equation

$$\frac{\partial T}{\partial t} = \sigma \left(\frac{\partial^2}{\partial x^2} + \frac{\partial^2}{\partial y^2} \right) T \tag{5.1}$$

5.1.2 Splitting

The splitting method for numerically solving the heat-flow equation is to replace the two-dimensional heat-flow equation by two one-dimensional equations, each of which is used on alternate time steps:

$$\frac{\partial T}{\partial t} = 2\,\sigma \frac{\partial^2 T}{\partial x^2} \qquad (\text{all } y) \tag{5.2}$$

$$\frac{\partial T}{\partial t} = 2\,\sigma \frac{\partial^2 T}{\partial y^2} \qquad (\text{all } x) \tag{5.3}$$

In equation (5.2) the heat conductivity σ has been doubled for flow in the x-direction and zeroed for flow in the y-direction. The reverse applies in equation (5.3). At odd moments in time heat flows according to (5.2) and at even moments in time it flows according to (5.3). This solution by alternation between (5.2) and (5.3) can be proved mathematically to converge to the solution to (5.1) with errors of the order of Δt. Hence the error goes to zero as Δt goes to zero. The motivation for splitting is the infeasibility of higher-dimensional implicit methods.

5.1.3 Full separation

Splitting can turn out to be much more accurate than might be imagined. In many cases there is *no* loss of accuracy. Then the method can be taken to an extreme limit. Think about a radical approach to equations (5.2) and (5.3) in which, instead of alternating back and forth between them at alternate time steps, what is done is to march (5.2) through all time steps. Then this intermediate result is used as an initial condition for (5.3), which is marched through all time steps to produce a final result. It might seem surprising that this radical method can produce the correct solution to equation (5.1). But if σ is a constant function of x and y, it does. The process is depicted in Figure 5.2 for an impulsive initial disturbance. A differential equation like (5.1) is said to be *fully separable* when the correct solution is obtainable by the radical method. It should not be too surprising that full separation works when σ is a constant, because then Fourier transformation may be used, and the two-dimensional solution $\exp[-\sigma\,(k_x^2 + k_y^2)t]$ equals the succession of one-dimensional solutions $\exp(-\sigma\,k_x^2 t)\ \exp(-\sigma\,k_y^2 t)$. It turns out, and will later be shown, that the condition required for applicability of full separation is that $\sigma\,\partial^2/\partial x^2$ should commute with $\sigma\,\partial^2/\partial y^2$, that is, the order of differentiation should be irrelevant. Technically

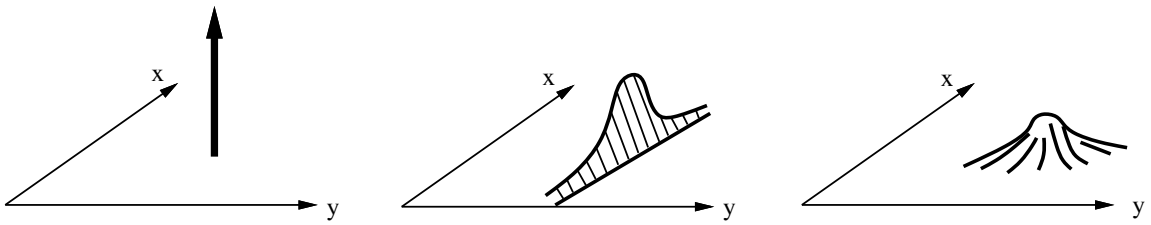

Figure 5.2: Temperature distribution in the (x, y)-plane beginning from a delta function (left). After heat is allowed to flow in the x-direction but not in the y-direction the heat is located in a "wall" (center). Finally allowing heat to flow for the same amount of time in the y-direction but not the x-direction gives the same symmetrical Gaussian result that would have been found if the heat had moved in x- and y-directions simultaneously (right). txz-temperature [NR]

there is also a boundary-condition requirement, but it creates no difficulty when the disturbance dies out before reaching a boundary.

Surprisingly, no notice is made of full separability in many textbooks on numerical solutions. Perhaps this is because the total number of additions and multiplications is the same whether a solution is found by splitting or by full separation. But as a practical matter, the cost of solving large problems does not mount up simply according to the number of multiplications. When the data base does not fit entirely into the random-access memory, as is almost the definition of a *large problem,* then each step of the splitting method demands that the data base be transposed, say, from (x, y) storage order to (y, x) storage order. Transposing requires no multiplications, but in many environments transposing would be by far the most costly part of the whole computation. So if transposing cannot be avoided, at least it should be reduced to a practical minimum.

There are circumstances which dictate a middle road between splitting and separation—for example, if σ were a slowly variable function of x or y. Then you might find that although $\sigma\,\partial^2/\partial x^2$ does not strictly commute with $\sigma\,\partial^2/\partial y^2$, it comes close enough that a number of time steps may be made with (5.2) before you transpose the data and switch over to (5.3). Circumstances like this one but with more geophysical interest arise with the wave-extrapolation equation that is considered next. The significance in seismology of the splitting and full separation concepts was first recognized by Brown [1983].

5.1.4 Application to lateral velocity variation

A circumstance in which the degree of noncommutativity of two differential operators has a simple physical meaning and an obviously significant geophysical application is the so-called monochromatic 15° wave-extrapolation equation in inhomogeneous media. Adding and subtracting a constant term to the unretarded 15° equation gives

us

$$\frac{\partial U}{\partial z} = \left[\frac{i\omega}{\bar{v}(z)} + i\omega \left(\frac{1}{v(x,z)} - \frac{1}{\bar{v}(z)} \right) - \frac{v(z)}{2\,i\omega} \frac{\partial^2}{\partial x^2} \right] U \qquad (5.4)$$
$$= (\text{ retardation } + \text{ thin lens } + \text{ diffraction}) \; U$$

Inspection of (5.4) shows that the retardation term commutes with the thin-lens term and with the free-space diffraction term. But the thin-lens term and the diffraction term do not commute with one another. In practice it seems best to split, doing the thin-lens part analytically and the diffraction part by the Crank-Nicolson method. Then stability is assured because the stability of each separate problem is known. Also, the accuracy of the analytic solution is an attractive feature. Now the question is, to what degree do these two terms commute?

The problem is just that of focusing a slide projector. Adjusting the focus knob amounts to repositioning the thin-lens term in comparison to the free-space diffraction term. There is a small range of knob positions over which no one can notice any difference, and a larger range over which the people in the back row are not disturbed by misfocus. Much geophysical data processing amounts to downward extrapolation of data. The lateral variation of velocity occurring in the lens term is known only to a limited accuracy. The application could be to determine $v(x)$ by the extrapolation procedure.

For long lateral spatial wavelengths the terms commute. Then diffraction may proceed in ignorance of the lateral variation in v. At shorter wavelengths the diffraction and lensing effects must be interspersed. So the real issue is not merely computational convenience but the interplay between data accuracy and the possible range for velocity in the underlying model.

5.1.5 Application to 3-d downward continuation

The operator for migration of zero-offset reflection seismic data in three dimensions is expandable to second order by Taylor series expansion to the so-called 15° approximation

$$\sqrt{\frac{(-i\omega)^2}{v^2} - \frac{\partial^2}{\partial x^2} - \frac{\partial^2}{\partial y^2}} \approx \frac{-i\omega}{v} - \frac{v}{-2i\omega} \frac{\partial^2}{\partial x^2} - \frac{v}{-2i\omega} \frac{\partial^2}{\partial y^2} \qquad (5.5)$$

The most common case is when v is slowly variable or independent of x and y. Then the conditions of full separation do apply. This is good news because it means that we can use ordinary 2-D wave-extrapolation programs for 3-D, doing the in-line data and the out-of-line data in either order. The bad news comes when we try for more accuracy. Keeping more terms in the Taylor series expansion soon brings in the cross term $\partial^4/\partial x^2 \partial y^2$. Such a term allows neither full separation nor splitting. Fortunately, present-day marine data-acquisition techniques are sufficiently crude in the out-of-line direction that there is little justification for out-of-line processing beyond the 15°

equation. Francis Muir had the good idea of representing the square root as

$$\sqrt{\frac{(-i\omega)^2}{v^2} - \frac{\partial^2}{\partial x^2} - \frac{\partial^2}{\partial y^2}} \approx \sqrt{\frac{(-i\omega)^2}{v^2} - \frac{\partial^2}{\partial x^2}} - \frac{v}{-2i\omega}\frac{\partial^2}{\partial y^2} \tag{5.6}$$

There may be justification for better approximations with land data. Fourier transformation of at least one of the two space axes will solve the computational problem. This should be a good approach when the medium velocity does not vary laterally so rapidly as to invalidate application of Fourier transformation.

5.1.6 Separability of 3-d migration (Jakubowicz)

In an operations environment, 3-D is much harder to cope with than 2-D. Therefore, it may be expedient to suppose that 3-D migration can be achieved merely by application of 2-D migration twice, once in the x-direction and once in the y-direction. The previous section would lead you to believe that such an expedient process would result in a significant degradation of accuracy. In fact, the situation is *much* better than might be supposed. It has been shown by Jakubowicz and Levin [1983] that, wonder of wonders, for a constant-velocity medium, the expedient process is exact.

The explanation is this: migration consists of more than downward continuation. It also involves imaging, that is, the selection of data at $t = 0$. In principle, downward continuation is first completed, for both the x and the y directions. After that, the imaging condition is applied. In the expedient process there are four steps: downward continuation in x, imaging, downward continuation in y, and finally a second imaging. Why it is that the expedient procedure gives the correct result seems something of a puzzle, but the validity of the result is easy to demonstrate.

First note that substitution of (5.7) into (5.8) gives (5.9) where

$$t_1^2 = t_0^2 + (x - x_0)^2/v^2 \tag{5.7}$$

$$t^2 = t_1^2 + (y - y_0)^2/v^2 \tag{5.8}$$

$$t^2 = t_0^2 + (x - x_0)^2/v^2 + (y - y_0)^2/v^2 \tag{5.9}$$

Equation (5.9) represents travel time to an arbitrary point scatterer. For a 2-D survey recorded along the y-axis, i.e., at constant x, equation (5.8) is the travel-time curve. In-line hyperbolas cannot be distinguished from sideswipe hyperbolas. 2-D migration with equation (5.8) brings the energy up to t_1. Subsequently migrating the other direction with equation (5.7) brings the energy up the rest of the way to t_0. This is the same result as the one given by the more costly 3-D procedure migrating with (5.9).

The Jakubowicz justification is somewhat more mathematical, but may be paraphrased as follows. First note that substitution of (5.10) into (5.11) gives (5.12) where

$$k_\tau^2 = \omega^2 - v^2 k_x^2 \tag{5.10}$$

$$k_z^2 = \frac{k_\tau^2}{v^2} - k_y^2 \tag{5.11}$$

$$k_z^2 = \frac{\omega^2}{v^2} - k_x^2 - k_y^2 \tag{5.12}$$

Two-dimensional Stolt migration over x may be regarded as a transformation from travel-time depth t to a pseudodepth τ by use of equation (5.10). The second two-dimensional migration over y may be regarded as a transformation from pseudodepth τ to true depth z by use of equation (5.11). The composite is the same as equation (5.12), which depicts 3-D migration.

The validity of the Jakubowicz result goes somewhat beyond its proof. Our two-dimensional geophysicist may be migrating other offsets besides zero offset. (In chapter 6 nonzero-offset data is migrated). If a good job is done, all the reflected energy moves up to the apex of the zero-offset hyperbola. Then the cross-plane migration can handle it if it can handle zero offset. So offset is not a problem. But can a good job be done of bringing all the energy up to the apex of the zero-offset hyperbola?

Difficulty arises when the velocity of the earth is depth-dependent, as it usually is. Then the Jakubowicz proof fails, and so does the expedient 3-D method. With a 2-D survey you have the problem that the sideswipe planes require a different migration velocity than the vertical plane. Rays propagating to the side take longer to reach the high-velocity media deep in the earth. So sideswipes usually require a lower migration velocity. If you really want to do three-dimensional migration with $v(z)$, you should forget about separation and do it the hard way. Since we know how to transpose the hard way really isn't much harder.

5.1.7 Separability in shot-geophone space

Reflection seismic data gathering is done on the earth's surface. One can imagine the appearance of the data that would result if the data were generated and recorded at depth, that is, with deeply buried shots and geophones. Such buried data could be synthesized from surface data by first downward extrapolating the geophones, then using the reciprocal principle to interchange sources and receivers, and finally downward extrapolating the surface shots (now the receivers). A second, equivalent approach would be to march downward in steps, alternating between shots and geophones. This latter approach is developed in chapter 6, but the result is simply stated by the equation

$$\frac{\partial U}{\partial z} = \left(\sqrt{\frac{(-i\omega)^2}{v(s)^2} - \frac{\partial^2}{\partial s^2}} + \sqrt{\frac{(-i\omega)^2}{v(g)^2} - \frac{\partial^2}{\partial g^2}} \right) U \tag{5.13}$$

The equivalence of the two approaches has a mathematical consequence. The shot coordinate s and the geophone coordinate g are independent variables, so the two square-root operators commute. Thus the same solution is obtained by splitting as by full separation.

5.1.8 Validity of the splitting and full-separation concepts

When Fourier transformation is possible, extrapolation operators are complex numbers like $e^{ik_z z}$. With complex numbers a and b there is never any question that $ab = ba$. Then both splitting and full separation are always valid, but the proof will be given only for a more general arrangement.

Suppose Fourier transformation has not been done, or could not be done because of some spatial variation of material properties. Then extrapolation operators are built up by combinations of the finite-differencing operators described in previous sections. Let $\mathbf{A}$ and $\mathbf{B}$ denote two such operators. For example, $\mathbf{A}$ could be a matrix containing the second x differencing operator. Seen as matrices, the boundary conditions of a differential operator are incorporated in the corners of the matrix. The bottom line is whether $\mathbf{AB} = \mathbf{BA}$, so the question clearly involves the boundary conditions as well as the differential operators.

Extrapolation forward a short distance can be done with the operator $(\mathbf{I} + \mathbf{A}\,\Delta z)$. In two-dimensional problems $\mathbf{A}$ was seen to be a four-dimensional matrix. For convenience the terms of the four-dimensional matrix can be arranged into a super-large, ordinary two-dimensional matrix. Implicit finite-differencing calculations gave extrapolation operators like $(\mathbf{I} + \mathbf{A}\,\Delta z)/(\mathbf{I} - \mathbf{A}\,\Delta z)$. Let $\mathbf{p}$ denote a vector where components of the vector designate the wavefield at various locations. As has been seen, the locations need not be constrained to the x-axis but could also be distributed throughout the (x, y)-plane. Numerical analysis gives us a matrix operator, say $\mathbf{A}$, which enables us to project forward, say,

$$\mathbf{p}(z + \Delta z) \quad = \quad \mathbf{A}_1\ \mathbf{p}(z) \tag{5.14}$$

The subscript on $\mathbf{A}$ denotes the fact that the operator may change with z. To get a step further the operator is applied again, say,

$$\mathbf{p}(z + 2\,\Delta z) \quad = \quad \mathbf{A}_2\ [\mathbf{A}_1\ \mathbf{p}(z)] \tag{5.15}$$

From an operational point of view the matrix $\mathbf{A}$ is never squared, but from an analytical point of view, it really is squared.

$$\mathbf{A}_2\ [\mathbf{A}_1\ \mathbf{p}(z)] \quad = \quad (\mathbf{A}_2\ \mathbf{A}_1)\ \mathbf{p}(z) \tag{5.16}$$

To march some distance down the z-axis we apply the operator many times. Take an interval $z_1 - z_0$, to be divided into N subintervals. Since there are N intervals, an error proportional to $1/N$ in each subinterval would accumulate to an unacceptable level by the time z_1 was reached. On the other hand, an error proportional to $1/N^2$ could only accumulate to a total error proportional to $1/N$. Such an error would disappear as the number of subintervals increased.

To prove the validity of splitting, we take $\Delta z = (z_1 - z_0)/N$. Observe that the operator $\mathbf{I} + (\mathbf{A} + \mathbf{B})\Delta z$ differs from the operator $(\mathbf{I} + \mathbf{A}\,\Delta z)(\mathbf{I} + \mathbf{B}\,\Delta z)$ by something in proportion to Δz^2 or $1/N^2$. So in the limit of a very large number of subintervals, the error disappears.

It is much easier to establish the validity of the full-separation concept. Commutativity is whether or not $\mathbf{A}\,\mathbf{B} = \mathbf{B}\,\mathbf{A}$. Commutativity is always true for scalars. With finite differencing the question is whether the two matrices commute. Taking $\mathbf{A}$ and $\mathbf{B}$ to be differential operators, commutativity is defined with the help of the family of all possible wavefields P. Then $\mathbf{A}$ and $\mathbf{B}$ are commutative if $\mathbf{A}\,\mathbf{B}\,P = \mathbf{B}\,\mathbf{A}\,P$.

The operator representing $\partial P/\partial z$ will be taken to be $\mathbf{A} + \mathbf{B}$. The simplest numerical integration scheme using the splitting method is

$$P(z_0 + \Delta z) \quad = \quad (\mathbf{I} + \mathbf{A}\,\Delta z)\,(\mathbf{I} + \mathbf{B}\,\Delta z)\,P(z_0) \tag{5.17}$$

Applying (5.17) in many stages gives a product of many operators. The operators $\mathbf{A}$ and $\mathbf{B}$ are subscripted with j to denote the possibility that they change with z.

$$P(z_1) \quad = \quad \prod_{j=1}^{N} \left[(\mathbf{I} + \mathbf{A}_j\,\Delta z)(\mathbf{I} + \mathbf{B}_j\,\Delta z)\right] P(z_0) \tag{5.18}$$

As soon as $\mathbf{A}$ and $\mathbf{B}$ are assumed to be commutative, the factors in (5.18) may be rearranged at will. For example, the $\mathbf{A}$ operator could be applied in its entirety before the $\mathbf{B}$ operator is applied:

$$P(z_1) \quad = \quad \left[\prod_{j=1}^{N} (\mathbf{I} + \mathbf{B}_j\,\Delta z)\right] \left[\prod_{j=1}^{N} (\mathbf{I} + \mathbf{A}_j\,\Delta z)\right] P(z_0) \tag{5.19}$$

Thus the full-separation concept is seen to depend on the commutativity of operators.

EXERCISES:

1 With a splitting method, Ma Zaitian (Ma [1981]) showed how very wide-angle representations may be implemented with successive applications of an equation like a 45° equation. This avoids the band matrix solving inherent in the high-order Muir expansion. Specifically, one chooses coefficients a_j and b_j, in the square-root fitting function

$$i\,k_z \quad = \quad \sum_{j=1}^{n-1} \frac{k_x^2\;b_j}{-i\omega + a_j\,ik_x} \tag{5.20}$$

The general n^{th}-order case is somewhat complicated, so your job is simply to find a_1, a_2, b_1, and b_2, to make the fitting function match the 45° equation.

2 Migrate a two dimensional data set with velocity v_1. Then migrate the migrated data set with a velocity v_2. Rocca pointed out that this double migration simulates a migration with a third velocity v_3. Using a method of deduction similar to the Jakubowicz deduction equations (5.10), (5.11), and (5.12) find v_3 in terms of v_1 and v_2.

3 Consider migration of zero-offset data $P(x, y, t)$ recorded in an area of the earth's surface plane. Assume a computer with a random access memory (RAM) large enough to hold several planes (any orientation) from the data volume. (The entire volume resides in slow memory devices). Define a migration algorithm by means of a program sketch. Your method should allow velocity to vary with depth.

5.2 RECURSIVE DIP FILTERS

Recursive filtering is a form of filtering where the output of the filter is fed back as an input. This can achieve a long impulse response for a tiny computational effort. It is particularly useful in computing a running mean. A running mean could be implemented as a low-pass filter in the frequency domain, but it is generally much better to avoid transform space. Physical space is cheaper, it allows for variable coefficients, and it permits a more flexible treatment of boundaries. Geophysical datasets are rarely stationary over long distances in either time or space, so recursive filtering is particularly helpful in statistical estimation.

The purpose of most filters is to make possible the observation of important weak events that are obscured by strong events. *One*-dimensional filters can do this only by the selection or rejection of *frequency* components. In *two* dimensions, a different criterion is possible, namely, selection by *dip.*

Dip filtering is a process of long-standing interest in geophysics (Embree, Burg, and Backus [1963]). Steep dips are often ground-roll noise. Horizontal dips can also be noise. For example, weak fault diffractions carry valuable information, but they may often be invisible because of the dominating presence of flat layers.

To do an ordinary dip-filtering operation ("pie slice"), you simply transform data into (ω, k)-space, multiply by any desired function of k/ω, and transform back. Pie-slice filters thus offer complete control over the filter response in k/ω dip space. While the recursive dip filters are not controlled so easily, they do meet the same general needs as pie-slice filters and offer the additional advantages of

- time- and space-variability
- causality
- ease of implementation
- orders of magnitude more economic than (ω, k)-implementation

The causality property offers an interesting opportunity during data recording. Water-velocity rejection filters could be built into the recording apparatus of a modern high-density marine cable.

5.2.1 Definition of a recursive dip filter

Let P denote raw data and Q denote filtered data. When seismic data is quasi-monochromatic, dip filtering can be achieved with spatial frequency filters. The table below shows filters with an adjustable cutoff parameter α.

Dip Filters for Monochromatic Data ($\omega \approx$ Const)	
Low Pass	High Pass
$Q = \frac{\alpha}{\alpha + k^2} P$	$Q = \frac{k^2}{\alpha + k^2} P$

To apply these filters in the space domain it is necessary only to interpret k^2 as the tridiagonal matrix $\mathbf{T}$ with $(-1, 2, -1)$ on the main diagonal. Specifically, for the low-pass filter it is necessary to solve a tridiagonal set of simultaneous equations like

$$(\alpha \mathbf{I} + \mathbf{T})\, \mathbf{q} = \alpha\, \mathbf{p} \tag{5.21}$$

in which $\mathbf{q}$ and $\mathbf{p}$ are column vectors whose elements denote different places on the x-axis. Previously, this was done while solving the heat-flow equation. To make the filter space-variable, the parameter α can be taken to depend on x so that $\alpha \mathbf{I}$ is replaced by an arbitrary diagonal matrix. It doesn't matter whether $\mathbf{p}$ and $\mathbf{q}$ are represented in the ω-domain or the t-domain.

Turn your attention from narrow-band data to data with a somewhat broader spectrum and consider

Dip Filters for Moderate Bandwidth Data ($\triangle\omega$)	
Low Pass	High Pass
$Q = \dfrac{\alpha}{\alpha + \dfrac{k^2}{-i\omega}} P$	$Q = \dfrac{\dfrac{k^2}{-i\omega}}{\alpha + \dfrac{k^2}{-i\omega}} P$

Naturally these filters can be applied to data of any bandwidth. However the filters are appropriately termed "dip filters" only over a modest bandwidth.

To understand these filters look in the (ω, k)-plane at contours of constant k^2/ω, i.e. $\omega \approx k^2$. Such contours, examples of which are shown in Figure 5.3, are curves of constant attenuation and constant phase shift. An interesting feature of these dip filters is that the low-pass and the high-pass filters constitute a pair of filters which

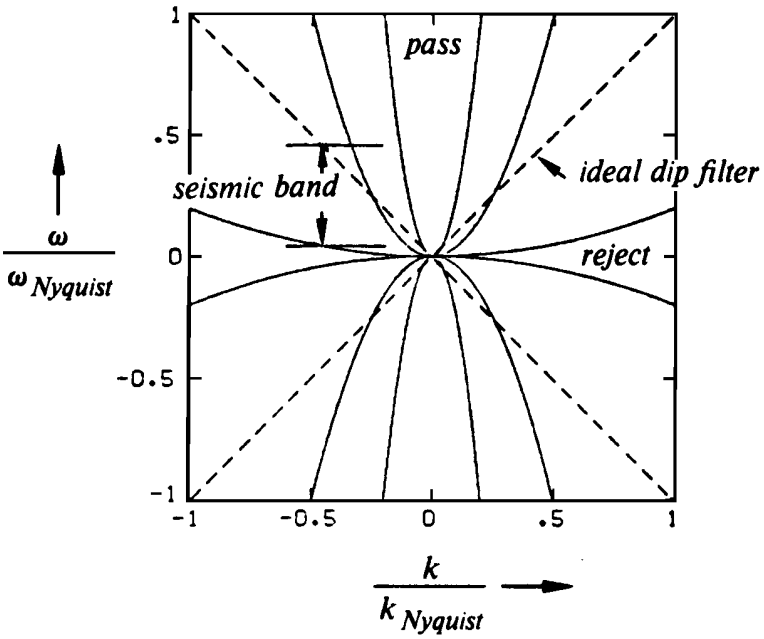

Figure 5.3: Constant-attenuation contours of dip filters. Over the seismic frequency band these parabolas may be satisfactory approximations to the dashed straight line. Pass/reject zones are indicated for the low-pass filter. (Hale) txz-dipfil [NR]

sum to unity. So nothing is lost if a dataset is partitioned by them in two. The high-passed part could be added to the low-passed part to recover the original dataset. Alternately, once the low-pass output is computed, it is much easier to compute the high-pass output, because it is just the input minus the low-pass. The low-pass filter has no phase shift in the pass zone, but there is time differentiation in the attenuation zone. This is apparent from the defining equation. The high-pass filter has no phase shift in the flat pass zone, but there is time integration in the attenuating zone.

5.2.2 Recursive-dip-filter implementation

Implementation of the moderate bandwidth dip filters is, again, a straightforward matter. For example, clearing fractions, the low-pass filter becomes

$$(-i\omega\alpha\,\mathbf{I}\;+\;\mathbf{T}\,)\,\mathbf{Q} \quad = \quad -i\omega\alpha\,\mathbf{P} \tag{5.22}$$

The main trick is to realize that the differentiation implied by $-i\omega$ is performed in a Crank-Nicolson sense. That is, terms not differentiated are averaged over adjacent values.

$$\mathbf{I}\,\frac{\alpha}{\Delta t}\,(\,\mathbf{q}_{t+1}\,-\,\mathbf{q}_t) \quad + \quad \mathbf{T}\,\frac{\mathbf{q}_{t+1}\,+\,\mathbf{q}_t}{2} \quad = \quad \frac{\alpha}{\Delta t}\,(\mathbf{p}_{t+1}\,-\,\mathbf{p}_t) \tag{5.23}$$

Gathering the unknowns to the left gives

$$\left(\frac{\alpha}{\Delta t}\,\mathbf{I}\,+\,\frac{1}{2}\,\mathbf{T}\right)\,\mathbf{q}_{t+1} \quad = \quad \left(\frac{\alpha}{\Delta t}\,\mathbf{I}\,-\,\frac{1}{2}\,\mathbf{T}\right)\,\mathbf{q}_t \quad + \quad \frac{\alpha}{\Delta t}\,(\mathbf{p}_{t+1}\,-\,\mathbf{p}_t) \tag{5.24}$$

Equation (5.24) is a tridiagonal system of simultaneous equations for the unknowns $\mathbf{q}_{t+1}$. The system may be solved recursively for successive values of t.

The parameter α determines the filter cutoff. It can be chosen to be any function of time and space. However, if the function is to vary extremely rapidly, then it may be necessary to incorporate some of the stability analysis that is developed in a later chapter for use with wave equations.

5.2.3 Side boundaries

Usually geophysicists wish that there were no boundaries on the sides, or that they were infinitely far away. There are two kinds of side conditions to think about, those in x, and those in k.

Often the side conditions on x are best approximated by zero-slope side conditions. It is possible to use more general side conditions because we have previously learned to solve any tridiagonal system of equations.

The side conditions in k-space relate to the steepest dips. A way to handle these dips is to use $\mathbf{T}/(\mathbf{I}-\beta\mathbf{T})$ to represent k^2. This introduces another adjustable parameter β, which must be kept less than 1/4.

5.2.4 Slicing pies

Naturally we may prefer true dip filters, that is, functions of k/ω instead of the functions of k^2/ω described above. But it can be shown that replacing k^2/ω in the above expressions by k^2/ω^2 gives recursions that are unstable.

Sharper pie slices (filters which are more strictly a rectangle function of k/ω), may be defined through a variety of approximation methods described by Hale and Claerbout [1983]. Generally, $|k|$ can be expanded in a power series in $\partial^2/\partial x^2$. If the approximation to $|k|$ is ensured positive, you can expect stability of the recursion that represents $|k|/i\omega$.

More simply, you might be willing to Fourier transform time or space, but not both. In the remaining dimension (the one not transformed) the required operation is a highpass or lowpass filter. This is readily implemented by a variety of techniques, such as the Butterworth filter.

5.2.5 Higher dimensionality

It is natural to think of a recursive three-dimensional low-pass dip filter as the functional form

$$\frac{\alpha}{\alpha \;+\; \frac{k_x^2 \;+\; k_y^2}{-\,i\,\omega}} \tag{5.25}$$

This, however, leads to an infeasible Crank-Nicolson situation. Multidimensional low-pass filtering *is* possible with

$$\left(\frac{\alpha_x}{\alpha_x \ + \ \frac{k_x^2}{-i\omega}} \right) \quad \left(\frac{\alpha_y}{\alpha_y \ + \ \frac{k_y^2}{-i\omega}} \right) \tag{5.26}$$

5.3 RETARDED COORDINATES

To examine running horses it may be best to jump on a horse. Likewise, to examine moving waves, it may be better to move along with them. So to describe waves moving downward into the earth we might abandon (x, z)-coordinates in favor of moving (x, z')-coordinates, where $z' = z + t\,v$.

An alternative to the moving coordinate system is to define *retarded coordinates* (x, z, t') where $t' = t - z/v$. The classical example of retarded coordinates is solar time. Time seems to stand still on an airplane that moves westward at the speed of the sun.

The migration process resembles the simulation of wave propagation in either a moving coordinate frame or a retarded coordinate frame. Retarded coordinates are much more popular than moving coordinates. Here is the reason: In solid-earth geophysics, velocity may depend on both x and z, but the earth doesn't change with time t during our seismic observations. In a moving coordinate system the velocity could depend on all three variables, thus unnecessarily increasing the complexity of the calculations. Fourier transformation is a popular means of solving the wave equation, but it loses most of its utility when the coefficients are nonconstant.

5.3.1 Definition of independent variables

The specific definition of retarded coordinates is a matter of convenience. Often the retardation is based on hypothetical rays moving straight down with velocity $\bar{v}(z)$. The definition of these coordinates has utility even in problems in which the earth velocity varies laterally, say $v(x, z)$, even though there may be no rays going exactly straight down. In principle, any coordinate system may be used to describe any circumstance, but the utility of the retarded coordinate system generally declines as the family of rays defining it departs more and more from the actual rays.

Despite the simple case at hand it is worthwhile to be somewhat formal and precise. Define the retarded coordinate system (t', x', z') in terms of ordinary Cartesian coordinates (t, x, z) by the set of equations

$$t' \quad = \quad t'(t,x,z) \quad = \quad t \ - \ \int_0^z \frac{dz}{\bar{v}(z)} \tag{5.27}$$

$$x' \quad = \quad x'(t,x,z) \quad = \quad x \tag{5.28}$$

$$z' \quad = \quad z'(t,x,z) \quad = \quad z \tag{5.29}$$

The purpose of the integral is to accumulate the travel time from the surface to depth z. The reasons to define (x', z') when it is just set equal to (x, z) are, first, to avoid confusion during partial differentiation and, second, to prepare for later work in which the family of rays is more general.

5.3.2 Definition of dependent variables

There are two kinds of *dependent* variables, those that characterize the medium and those that characterize the waves. The medium is characterized by its velocity v and its reflectivity c. The waves are characterized by using U for an upcoming wave, D for a downgoing wave, P for the pressure, and Q for a modulated form of pressure. Let us say $P(t, x, z)$ is the mathematical function to find pressure, given (t, x, z); and $P'(t', x', z')$ is the mathematical function given (t', x', z'). The statement that the two mathematical functions P and P' both refer to the same physical variable is this:

$$\begin{aligned} P(t, x, z) &= P'[t'(t, x, z),\ x'(t, x, z),\ z'(t, x, z)] \\ P(t, x, z) &= P'(t', x', z') \end{aligned} \tag{5.30}$$

Obviously there are analogous expressions for the other dependent variables and medium parameters like velocity $v(x, z)$.

5.3.3 The chain rule and the high frequency limit

The familiar partial-differential equations of physics come to us in (t, x, z)-space. The chain rule for partial differentiation will convert the partial derivatives to (t', x', z')-space. For example, differentiating (5.30) with respect to z gives

$$\frac{\partial P}{\partial z} = \frac{\partial P'}{\partial t'}\frac{\partial t'}{\partial z} + \frac{\partial P'}{\partial x'}\frac{\partial x'}{\partial z} + \frac{\partial P'}{\partial z'}\frac{\partial z'}{\partial z} \tag{5.31}$$

Using (5.27), (5.28) and (5.29) to evaluate the coordinate derivatives gives

$$\frac{\partial P}{\partial z} = -\frac{1}{\bar{v}}\frac{\partial P'}{\partial t'} + \frac{\partial P'}{\partial z'} \tag{5.32}$$

There is nothing special about the variable P in (5.31) and (5.32). We could as well write

$$\frac{\partial}{\partial z} = -\frac{1}{\bar{v}}\frac{\partial}{\partial t'} + \frac{\partial}{\partial z'} \tag{5.33}$$

where the left side is for operation on functions that depend on (t, x, z) and the right side is for functions of (t', x', z'). Differentiating twice gives

$$\frac{\partial^2}{\partial z^2} = \left(\frac{-1}{\bar{v}}\frac{\partial}{\partial t'} + \frac{\partial}{\partial z'}\right)\left(\frac{-1}{\bar{v}}\frac{\partial}{\partial t'} + \frac{\partial}{\partial z'}\right) \tag{5.34}$$

Using the fact that the velocity is always time-independent results in

$$\frac{\partial^2}{\partial z^2} \quad = \quad \frac{1}{\bar{v}^2}\,\frac{\partial^2}{\partial t'^2} \;-\; \frac{2}{\bar{v}}\,\frac{\partial^2}{\partial t'\,\partial z'} \;+\; \frac{\partial^2}{\partial z'^2} \;+\; \frac{1}{\bar{v}^2}\,\frac{d\bar{v}}{dz'}\,\frac{\partial}{\partial t'} \tag{5.35}$$

Except for the rightmost term with the square brackets it could be said that "squaring" the operator (5.33) gives the second derivative. This last term is almost always neglected in data processing. The reason is that its effect is similar to the effect of other first-derivative terms with material gradients for coefficients. Such terms, cause amplitudes to be more carefully computed. that all such terms should be included, from the beginning.

5.3.4 Fourier transforms in retarded coordinates

Given a pressure field $P(t,x,z)$, we may Fourier transform it with respect to any or all of its independent variables (t,x,z). Likewise, if the pressure field is specified in retarded coordinates, we may Fourier transform with respect to (t',x',z'). Since the Fourier dual of (t,x,z) is (ω,k_x,k_z), it seems appropriate for the dual of (t',x',z') to be $(\omega',k_x{}',k_z{}')$. Now the question is, how are $(\omega',k_x{}',k_z{}')$ related to the familiar (ω,k_x,k_z)? The answer is contained in the chain rule for partial differentiation. Any expression like (5.33)

$$\frac{\partial}{\partial z} \quad = \quad -\,\frac{1}{\bar{v}}\,\frac{\partial}{\partial t'} \;+\; \frac{\partial}{\partial z'}$$

on Fourier transformation says

$$i\,k_z \quad = \quad -\,\frac{-\,i\,\omega'}{\bar{v}} \;+\; i\,k_z{}' \tag{5.36}$$

Computing all the other derivatives, we have the transformation

$$\omega \quad = \quad \omega' \tag{5.37}$$

$$k_x \quad = \quad k_x{}' \tag{5.38}$$

$$k_z \quad = \quad k_z{}' \;+\; \frac{\omega'}{\bar{v}} \tag{5.39}$$

Recall the dispersion relation for the scalar wave equation:

$$\frac{\omega^2}{v^2} \quad = \quad k_x^2 \;+\; k_z^2 \tag{5.40}$$

Performing the substitutions from (5.37), (5.38) and (5.39) into (5.40) we have the expression of the scalar wave equation in retarded time, namely,

$$\left(\frac{\omega'}{v}\right)^2 \quad = \quad k_x{}'^2 \;+\; \left(k_z{}' \;+\; \frac{\omega'}{\bar{v}}\right)^2 \tag{5.41}$$

These two dispersion relations are plotted in Figure 5.4 for the retardation velocity chosen equal to the medium velocity. Figure 5.4 graphically illustrates that retarda-

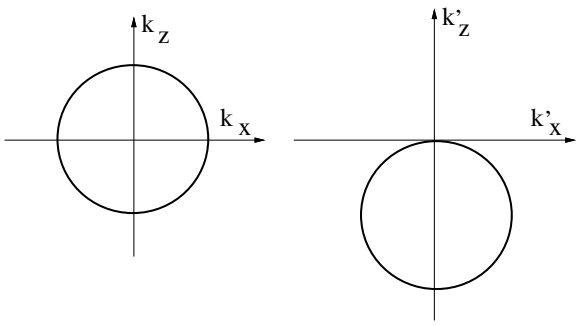

Figure 5.4: Dispersion relation of the wave equation in usual coordinates (left) and retarded time coordinates (right). txz-rdisper [NR]

tion can reduce the cost of finite-difference calculations. Waves going straight down are near the top of the dispersion curve (circle). The effect of retardation is to shift the circle's top down to the origin. Discretizing the x- and z-axes will cause spatial frequency aliasing on them. The larger the frequency ω, the larger the circle. Clearly the top of the shifted circle is further from folding. Alternately, Δz may be increased (for the sake of economy) before k'_z exceeds the Nyquist frequency $\pi/\Delta z$.

5.3.5 Interpretation of the modulated pressure variable Q

Earlier a variable Q was defined from the pressure P by the equation

$$P(\omega) \quad = \quad Q(\omega) \; \exp \left[\; i\omega \int_0^z \frac{dz}{\bar{v}(z)} \; \right] \tag{5.42}$$

The right side is a product of two functions of ω. At constant velocity (5.42) is expressed as

$$P(\omega) \quad = \quad Q(\omega) \; e^{i\omega z/v} \quad = \quad Q(\omega) \; e^{i\omega t_0} \tag{5.43}$$

In the time domain $e^{i\omega t_0}$ becomes a delta function $\delta(t \; - \; t_0)$. Equation (5.43) is a product in the frequency domain, so in the time domain it is the convolution

$$\begin{aligned} p(t) &= q(t) * \delta(t \; - \; z/v) \\ &= q(t \; - \; z/v) \\ &= q(t') \end{aligned} \tag{5.44}$$

This confirms that the definition of a dependent variable Q is equivalent to introducing retarded time t'.

5.3.6 Einstein's special relativity theory

There is no known application of Einstein's theory of special relativity to seismic imaging. But some of the mathematical methods are related, and now is the appropriate time to take a peek at this famous theory.

In 1887 the Michelson-Morley interferometer experiment established with high accuracy that light travels in all directions at the same speed, day and night, winter and summer. We have seen that the dispersion relation of the scalar wave equation is a circle centered at the origin, meaning that waves go the same speed in all directions. But if the coordinate system is moving with respect to the medium, then the dispersion relation loses directional symmetry. For light propagating in the vacuum of outer space, there seems to be no natural reference coordinate system. If the earth is presumed to be at rest in the summer, then by winter, the earth is moving around the sun in the opposite direction. The summer coordinates relate to the winter coordinates by something like $x' = x - 2\,v_{\text{earth}}t$. While analysis of the Michelson-Morley experiment shows that such motion should have a measurable asymmetry, measurements show that the predicted asymmetry is absent. Why? One theory is the "ether" theory. Ether is a presumed substance that explains the paradox of the Michelson-Morley experiment. It is presumed to be of minuscule density and viscosity, allowing us to imagine that it is somehow dragged around the earth in such a way that earthbound experimenters are always moving at the same speed as it is. Other measurements, however, also contradict the presumption of ether. Just as wind refracts atmospheric sound waves, ether should cause a measurable refraction of starlight, but this is not observed.

Einstein's explanation of the experiments is based on a mathematical fact that you can easily verify. Let a coordinate frame be defined by

$$z' = z - \frac{v\,t}{\sqrt{1 - v^2/c^2}} \tag{5.45}$$

$$x' = x \tag{5.46}$$

$$t' = \frac{t - \frac{v}{c^2}\,z}{\sqrt{1 - v^2/c^2}} \tag{5.47}$$

The amazing thing about this transformation, which you can easily prove, is that it converts the equation $P_{xx} + P_{zz} = c^{-2}P_{tt}$ to the equation $P_{x'x'} + P_{z'z'} = c^{-2}P_{t't'}$. The transformed wave equation is independent of velocity v which is what led Einstein to his surprising conclusions.

5.4 FINITE DIFFERENCING IN (t, x, z)-SPACE

Much, if not most, production migration work is done in $(t,\ x,\ z)$-space. To avoid being overwhelmed by the complexity of this three-dimensional space, we will first look at migration in $(z,\ t)$-space for fixed k_x.

5.4.1 Migration in (z, t)-space

Migration and data synthesis may be envisioned in (z', t')-space on the following table, which contains the upcoming wave U:

t' \ z'					
	c_0				
	u_1	c_1			
	u_2		c_2		
	u_3			c_3	
	u_4				c_4
	0	0	0	0	0

(5.48)

In this table the observed upcoming wave at the earth's surface $z' = 0$ is denoted by u_t. The migrated section, denoted by c_t, is depicted along the diagonal because the imaging condition of exploding reflectors at time $t = 0$ is represented in retarded space as

$$z' = z \tag{5.49}$$

$$t' = t + z/v \qquad (+ \text{ for up}) \tag{5.50}$$

$$0 = t = t' - z'/v \tag{5.51}$$

The best-focused migration need not fall on the 45° line as depicted in (5.48); it might be on any line or curve as determined by the earth velocity. This curve forms the basis for velocity determination. You couldn't determine velocity this way in the frequency-domain.

The equation for upcoming waves U in retarded coordinates (t', x', z') is

$$\frac{\partial^2 U}{\partial z' \, \partial t'} = -\frac{v}{2} \frac{\partial^2 U}{\partial x'^2} \tag{5.52}$$

Next, Fourier transform the x-axis. This assumes that v is a constant function of x and that the x-dependence of U is the sinusoidal function $\exp(ik_x x)$. Thus,

$$0 = \left(\frac{v}{2} k_x^2 - \frac{\partial^2}{\partial z' \, \partial t'} \right) U \tag{5.53}$$

Now this partial-differential equation will be discretized with respect to t' and z'. Matrix notation will be used, but the notation does not refer to matrix algebra. Instead the matrices refer to differencing stars that may be placed on the $(t',\ z')$-plane of (5.48). Let $*$ denote convolution in $(z,\ t)$-space. A succession of derivatives is really a convolution, so the concept of $(\partial/\partial z)(\partial/\partial t) = \partial^2/\partial z \partial t$ is expressed by

$$\begin{bmatrix} -1 & +1 \end{bmatrix} \ * \ \begin{bmatrix} -1 \\ +1 \end{bmatrix} \ = \ \begin{bmatrix} 1 & -1 \\ -1 & 1 \end{bmatrix} \tag{5.54}$$

Thus, the differenced form of (5.53) is

$$0 \ = \ \left\{ \frac{v}{2} \frac{\Delta z' \, \Delta t'}{4} \ k_x^2 \ \begin{bmatrix} 1 & 1 \\ 1 & 1 \end{bmatrix} \ - \ \begin{bmatrix} 1 & -1 \\ -1 & 1 \end{bmatrix} \right\} * U \tag{5.55}$$

The 1/4 enters in because the average of U is taken over four places on the mesh.

The sum of the two operators always has $|b| \ \geq \ |s|$ in the form

$$0 \ = \ \begin{bmatrix} s & b \\ b & s \end{bmatrix} \ * \ U \tag{5.56}$$

Now the differencing star in (5.56) will be used to fill the table (5.48) with values for U.

Given the three values of U in the boxes, a missing one, M, may be determined by either of the implied two operations

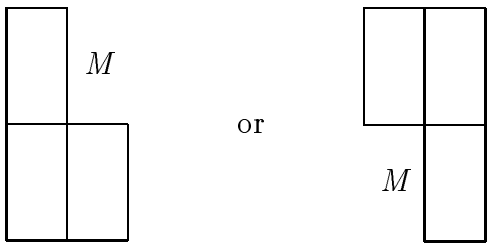

(5.57)

It turns out that because $|b| \ \geq \ |s|$, the implied filling operations by

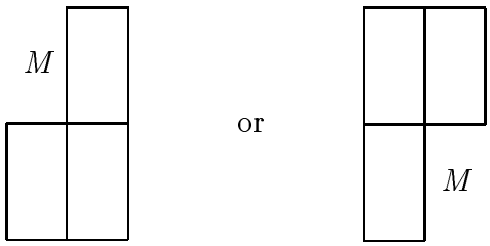

(5.58)

are unstable. It is obvious that there would be a zero-divide problem if s were equal to 0, and it is not difficult to do the stability analysis that shows that (5.58) causes exponential growth of small disturbances.

It is a worthwhile exercise to make the zero-dip assumption ($k_x = 0$) and use the numerical values in the operator of (5.56) to fill in the elements of the table (5.48). It will be found that the values of u_t move laterally in z across the table with no change, predicting, as the table should, that $c_t = u_t$. Slow change in z suggests that we have oversampled the z-axis. In practice, effort is saved by sampling the z-axis with fewer points than are used to sample the t-axis.

5.4.2 (t,x,z)-Space, 15 degree Diffraction Program

The easiest way to understand 15° migration in $(t,\ x,\ z)$-space is to refer to the $(z,\ t)$-space migration. Instead of a scalar function $U(k_x)$, we use $\mathbf{u}$, a vector whose components u_j measure pressure at $x = j\,\Delta x$. Think of k_x^2 as a tridiagonal matrix, call it $\mathbf{T}$, with $(-1, 2, -1)$ on the main diagonal. Note that k_x^2 is positive, and that $\mathbf{T}$ is a positive definite matrix with a positive element on its main diagonal. Take equation (5.55) and use α to denote the left constant. This gives

$$0 \;=\; \left\{ \alpha\mathbf{T} \begin{bmatrix} \mathbf{I} & \mathbf{I} \\ \mathbf{I} & \mathbf{I} \end{bmatrix} \;-\; \begin{bmatrix} \mathbf{I} & -\mathbf{I} \\ -\mathbf{I} & \mathbf{I} \end{bmatrix} \right\} * \mathbf{u} \;=\; \begin{bmatrix} \alpha\mathbf{T} - \mathbf{I} & \alpha\mathbf{T} + \mathbf{I} \\ \alpha\mathbf{T} + \mathbf{I} & \alpha\mathbf{T} - \mathbf{I} \end{bmatrix} * \mathbf{u} \qquad (5.59)$$

```
# Time Domain 15-degree Diffraction Movie
# Star:          w=p(t  ,z)      y=p(t  ,z+1)
#%Star:          u=p(t+1,z)      v=p(t+1,z+1)
subroutine test()
real p(37,96),u(36),w(36),v(36),y(36),e(36),f(36),d(36),z(96),alfa,beta
real apb, amb, diag, offdi, dd
integer i,ix,nx,iz,nz,it,nt,esize
nx = 36;   nz = 96;   nt = 96;  esize=4
to history:     integer esize, n1:nx+1, n2:nz, n3:nz/2
call hclose()
alfa = .125             # v*dz*dt/(8*dx*dx)
beta = .140             # accurate x derivative parameter; simplest case b=0.
do iz = 1,nz { do ix=1,nx { p(ix,iz) = 0.}}
do iz = nz/5, nz, nz/4                  # Set up initial model
        do it= 1,15                     # of 4 band limited
                do ix= 1,4              # "point" scatterers.
                        p(ix,it+iz) = (5.-ix)*(8-it)*exp(-.1*(it-8)**2)
apb = alfa+beta;        amb = alfa-beta # tridiagonal coefficients
diag = 1.+2.*amb;   offdi = -amb
do iz= nz, 2, -2 {                      # Climb up in steps of 2 z-levels
        do i=1,nz{ p(nx+1,i)=0}; p(nx+1,iz)=1.  # Pointer to current z-level
        call srite('out', p, nz*(nx+1)*4)
        do ix= 1, nx
                { u(ix) = p(ix,iz-1);   v(ix) = u(ix) }
        do it= iz, nt {
                do ix= 1, nx            #update the differencing star
                        { w(ix) = u(ix);  y(ix) = v(ix);  v(ix) = p(ix,it) }
                dd = (1.-apb)*(v(1)+w(1))+apb*(v(2)+w(2))
                d(1) = dd-diag*y(1)-offdi*(y(1)+y(2))
                do ix= 2, nx-1 {
                        dd    = (1.-2.*apb)*(v(ix)+w(ix))
                        dd    = dd + apb*(v(ix-1)+w(ix-1)+v(ix+1)+w(ix+1))
                        d(ix) = dd-diag*y(ix)-offdi*(y(ix-1)+y(ix+1))   }
                dd = (1.-apb)*(v(nx)+w(nx))+apb*(v(nx-1)+w(nx-1))
                d(nx) = dd-diag*y(nx)-offdi*(y(nx)+y(nx-1))
                call rtris(nx,diag+offdi,offdi,diag,offdi,diag+offdi,d,u)
                do ix= 1, nx
                        p(ix,it) = u(ix)
                }
        }
return; end
```

Consider a modeling program. It begins down inside the earth with the differencing star on the right side of (5.57). Solving (5.59) for the unknown $\mathbf{u}_{t'+1,z'}$ and dropping all primes yields

$$(\alpha\mathbf{T} + \mathbf{I})\,\mathbf{u}_{t+1,z} \;=\; -\,[(\alpha\mathbf{T} + \mathbf{I})\,\mathbf{u}_{t,z+1} \;+\; (\alpha\mathbf{T} - \mathbf{I})(\mathbf{u}_{t,z} \;+\; \mathbf{u}_{t+1,z+1})] \qquad (5.60)$$

First, evaluate the expression on the right. The left side is a tridiagonal system to be solved for the unknown $\mathbf{u}_{t+1,z}$. Allowable sequences in which (5.60) may be applied are dictated by the differencing star on the right side of (5.57).

Heeding the earlier remark that with waves of modest dip, the z'-axis need not be sampled so densely as the t'-axis, we do a computation that skips alternate levels of z'. The specific order chosen in the computer program `time15` is indicated by the numbers in the following table:

t'			z'	
	c_0	c_0		
	5	c_1		
	6	c_2	c_2	
	7	2	c_3	
	8	3	c_4	c_4
	9	4	1	c_5

(5.61)

An inescapable practical problem shown in the table when the number of points in t'-space is not exactly equal that in z'-space is that the earth image must be *interpolated* along a diagonal on the mesh. The crude interpolation in (5.61) illustrates the assumption that the wave field changes rapidly in t' but slowly in z', i.e. the small-angle assumption.

Figure 5.5 shows the last frame in the movie produced by the test program. Exercise 1 suggests minor changes to the program `time15` to convert it from diffraction to migration. As modified, the program is essentially the original wave equation migration program introduced by Johnson and Claerbout [1971] and Doherty and Claerbout [1972].

5.4.3 You Can't Time Shift in the Time Domain.

You might wish to do migration in $(x,\ z,\ t)$-space with lateral velocity variation. Then the thin-lens stage would be implemented by time shifting instead of by multiplying by $\exp\{i\omega\,[v(x,\ z)^{-1} - \bar{v}(z)^{-1}]\Delta z\}$. Time shifting is a delightfully easy operation when

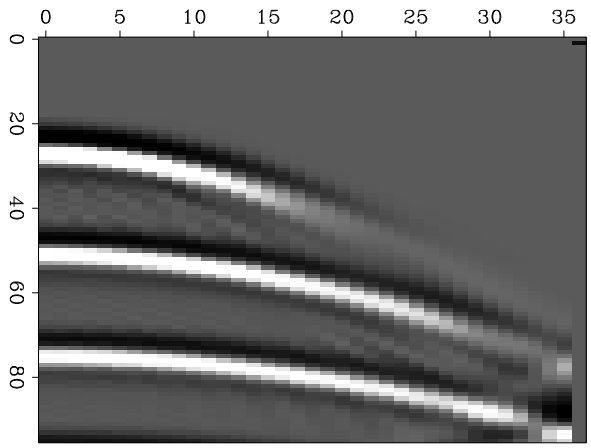

Figure 5.5: Diffractions in the last frame of the downward-continuation movie. txz-diffr [ER]

what is needed is to shift data by an integral number of sample units. Repetitive time shifting by a fractional number of digital units, however, is a nightmare. Multipoint interpolation operators are required. Even then, pulses tend to disperse. So the lens term is probably best left in the frequency domain.

5.4.4 (t,x,z)-Space, 45 degree equation

The 45° migration is a little harder than the 15° migration because the operator in the time domain is higher order, but the methods are similar to those of the 15° equation and the recursive dip filter. The straightforward approach is just to write down the differencing stars. When I did this kind of work I found it easiest to use the Z-transform approach where $1/(-i\omega\Delta t)$ is represented by the bilinear transform $\frac{1}{2}(1+Z)/(1-Z)$. There are various ways to keep the algebra bearable. One way is to bring all powers of Z to the numerator and then collect powers of Z. Another way, called the integrated approach, is to keep $1/(1-Z)$ with some of the terms. Terms including $1/(1-Z)$ are represented in the computer by buffers that contain the sum from infinite time to time t. The Z-transform approach systematizes the stability analysis.

EXERCISES:

1 Alter the program `time15` so that it does migration. The delta-function inputs should turn into approximate semicircles.

2 Perform major surgery on the program `time15` so that it becomes a low-pass dip filter.

Figure 5.6: The program `time15` was used to create synthetic data from a more complicated model. The three frames depict three depths. The leftmost channel of each frame depicts the depth of the frame. txz-gas [ER]

3 Consider a 45° migration program in the space of $(z,\ t, k_x)$. Find the coefficients in a 6-point differencing star, three points in time and two points in depth. For simplicity, take $v = 1$, $\Delta t = 1$, and $\Delta z = 1$. Suppose this analysis were transformed into the x-domain ($\Delta x = 1$) by replacing k_x^2 with $\mathbf{T}$. What set of tridiagonal equations would have to be solved?

5.5 INTRODUCTION TO STABILITY

Experience shows that as soon as you undertake an application that departs significantly from textbook situations, stability becomes a greater concern than accuracy. Stability, or its absence, determines whether the goal is achievable at all, whereas accuracy merely determines the price of achieving it. Here we will look at the stability of the heat-flow equation with real and with imaginary heat conductivity. Since the latter case corresponds to seismic migration, these two cases provide a useful background for stability analysis.

Most stability analysis is based on Fourier transformation. More simply, single sinusoidal or complex exponential trial solutions are examined. If a method becomes unstable for any frequency, then it will be unstable for any realistic case, because realistic functions are just combinations of all frequencies. Begin with the sinusoidal function

$$P(x) \quad = \quad P_0\ e^{i\,k\,x} \tag{5.62}$$

The second derivative is

$$\frac{\partial^2 P}{\partial x^2} \quad = \quad -\,k^2\,P \tag{5.63}$$

An expression analogous to the second difference operator defines $\hat{k}$:

$$\frac{\delta^2 P}{\delta x^2} \quad = \quad \frac{P(x\ +\ \Delta x)\ -\ 2\,P(x)\ +\ P(x\ -\ \Delta x)}{\Delta x^2} \tag{5.64}$$

$$= \quad -\hat{k}^2\,P \tag{5.65}$$

Ideally $\hat{k}$ should equal k. Inserting the complex exponential (5.62) into (5.64) gives an expression for $\hat{k}$:

$$-\ \hat{k}^2\,P \quad = \quad \frac{P_0}{\Delta x^2}\ \left[\ e^{ik(x+\Delta x)}\ -\ 2\,e^{ik\,x}\ +\ e^{ik(x-\Delta x)}\right] \tag{5.66}$$

$$(\hat{k}\,\Delta x)^2 \quad = \quad 2\ [1\ -\ \cos(k\Delta x)] \tag{5.67}$$

It is a straightforward matter to make plots of (5.67) or its square root. The square root of (5.67), through the half-angle trig identity, is

$$\hat{k}\,\Delta x \quad = \quad 2\ \sin\frac{k\,\Delta x}{2} \tag{5.68}$$

Series expansion shows that $\hat{k}$ matches k well at low spatial frequencies. At the Nyquist frequency, defined by $k\Delta x = \pi$, the value of $\hat{k}\Delta x = 2$ is a poor approximation

to π. As with any Fourier transform on the discrete domain, $\hat{k}$ is a periodic function of k above the Nyquist frequency. Although k ranges from minus infinity to plus infinity, $\hat{k}^2$ is compressed into the range zero to four. The limits to the range are important since instability often starts at one end of the range.

5.5.1 Stability of the explicit heat-flow equation

Begin with the heat-flow equation and Fourier transform over space. Thus $\partial^2/\partial x^2$ becomes simply $-k^2$, and

$$\frac{\partial q}{\partial t} \quad = \quad -\frac{\sigma}{c}\, k^2\, q \tag{5.69}$$

Finite differencing explicitly over time gives an equation that is identical in form to the inflation-of-money equation:

$$\frac{q_{t+1} - q_t}{\Delta t} \quad = \quad -\frac{\sigma}{c}\, k^2\, q_t \tag{5.70}$$

$$q_{t+1} \quad = \quad \left(1 - \frac{\sigma\, \Delta t}{c}\, k^2\right)\, q_t \tag{5.71}$$

For stability, the magnitude of q_{t+1} should be less than or equal to the magnitude of q_t. This requires the factor in parentheses to have a magnitude less than or equal to unity. The dangerous case is when the factor is more negative than -1. There is instability when $k^2 > 2c/(\sigma\, \Delta t)$. This means that the high frequencies are diverging with time. The explicit finite differencing on the time axis has caused disaster for short wavelengths on the space axis. Surprisingly, this disaster can be recouped by differencing the space axis coarsely enough! The second space derivative in the Fourier transform domain is $-\,k^2$. When the x-axis is discretized it becomes $-\hat{k}^2$. So, to discretize (5.69), (5.70) and (5.71), just replace k by $\hat{k}$. Equation (5.68) shows that $\hat{k}^2$ has an upper limit of $\hat{k}^2 \;=\; 4/\Delta x^2$ at the Nyquist frequency $k\Delta x = \pi$. Finally, the factor in (5.71) will be less than unity and there will be stability if

$$\hat{k}^2 \quad = \quad \frac{4}{\Delta x^2} \quad \leq \quad \frac{2\, c}{\sigma\, \Delta t} \tag{5.72}$$

Evidently instability can be averted by a sufficiently dense sampling of time compared to space. Such a solution becomes unbearably costly, however, when the heat conductivity $\sigma(x)$ takes on a wide range of values. For problems in one space dimension, there is an easy escape in implicit methods. For problems in higher-dimensional spaces, explicit methods must be used.

5.5.2 Explicit 15 degree migration equation

We saw that the retarded 15° wave-extrapolation equation is like the heat-flow equation with the exception that the heat conductivity σ must be replaced by the purely imaginary number i. The amplification factor (the magnitude of the factor in parentheses in equation (5.71)) is now the square root of the sum squared of real and

imaginary parts. Since the real part is already one, the amplification factor exceeds unity for all nonzero values of k^2. The resulting instability is manifested by the growth of dipping plane waves. The more dip, the faster the growth. Furthermore, discretizing the x-axis does not solve the problem.

5.5.3 Implicit equations

Recall that the inflation-of-money equation

$$q_{t+1} \ - \ q_t \quad = \quad r \ q_t \tag{5.73}$$

is a simple explicit finite differencing of the differential equation $dq/dt \ \approx \ q$. And recall that a better approximation to the differential equation is given by the Crank-Nicolson form

$$q_{t+1} \ - \ q_t \quad = \quad r \ \frac{q_{t+1} \ + \ q_t}{2} \tag{5.74}$$

that may be rearranged to

$$\left(1 \ - \ \frac{r}{2} \right) q_{t+1} \quad = \quad \left(1 \ + \ \frac{r}{2} \right) q_t \tag{5.75}$$

or

$$\frac{q_{t+1}}{q_t} \quad = \quad \frac{1 \ + \ r/2}{1 \ - \ r/2} \tag{5.76}$$

The amplification factor (5.76) has magnitude less than unity for all negative r values, even r equal to minus infinity. Recall that the heat-flow equation corresponds to

$$r \quad = \quad - \ \frac{\sigma \ \Delta t}{c} \ k^2 \tag{5.77}$$

where k is the spatial frequency. Since (5.76) is good for all negative r, the heat-flow equation, implicitly time-differenced, is good for all spatial frequencies k. The heat-flow equation is stable whether or not the space axis is discretized (then $k \ \rightarrow \ \hat{k}$) and regardless of the sizes of Δt and Δx. Furthermore, the 15° wave-extrapolation equation is also unconditionally stable. This follows from letting r in (5.76) be purely imaginary: the amplification factor (5.76) then takes the form of some complex number $1 + r/2$ divided by its complex conjugate. Expressing the complex number in polar form, it becomes clear that such a number has a magnitude exactly equal to unity. Again there is unconditional stability.

At this point it seems right to add a historical footnote. When finite-difference migration was first introduced many objections were raised on the basis that the theoretical assumptions were unfamiliar. Despite these objections finite-difference migration quickly became popular. I think the reason for its popularity was that, compared to other methods of the time, it was a gentle operation on the data. More specifically, since (5.76) is of exactly unit magnitude, the output has the same (ω, k)-spectrum as the input. There may be a wider lesson to be learned from this experience: any process acting on data should do as little to the data as possible.

5.5.4 Leapfrog equations

The leapfrog method of finite differencing, it will be recalled, requires expressing the time derivative over two time steps. This keeps the centers of the differencing operators in the same place. For the heat-flow equation Fourier-transformed over space,

$$\frac{q_{t+1} - q_{t-1}}{2\,\Delta t} \quad = \quad -\frac{\sigma}{c}\, k^2\, q_t \tag{5.78}$$

It is a bit of a nuisance to analyze this equation because it covers times $t-1$, t, and $t+1$ and requires slightly more difficult analytical techniques. Therefore, it seems worthwhile to state the results first. The result for the heat-flow equation is that the solution always diverges. The result for the wave-extrapolation equation is much more useful: there is stability provided certain mesh-size restrictions are satisfied, namely, Δz must be less than some factor times Δx^2. This result is not exciting in one space dimension (where implicit methods seem ideal), but in higher-dimensional space, such as in the so-called 3-D prospecting surveys, we may be thankful to have the leapfrog method.

The best way to analyze equations like (5.78) which range over three or more time levels is to use Z-transform filter analysis. Converted to a Z-transform filter problem, the question posed by (5.78) becomes whether the filter has zeroes inside (or outside) the unit circle. Z-transform stability analysis is described elswhere Such analysis is necessary for all possible numerical values of k^2. Its result is that there is always trouble if k^2 ranges from zero to infinity. But with the wave-extrapolation equation, instability can be avoided with certain mesh-size restrictions, because $(\hat{k}\,\Delta x)^2$ lies between zero and four.

5.5.5 Tridiagonal equation solver

The tridiagonal algorithm is stable for all positive definite matrices. If you have any problems with the tridiagonal solver, you should question the validity of your problem formulation. What is there about your application that seems to demand division by zero?

Chapter 6

Offset, another dimension

Earlier chapters have assumed that the shot and the geophone are located in the same place. The reality is that there is often as much as a 3-km horizontal separation between them. The 3-km offset is comparable to the depth of many petroleum reservoirs.

Offset is another *dimension* in the analysis of data. At the time of writing, this dimension is often represented in field operations by about 48 channels. No one seems to believe, however, that 48 channels is enough. Recording systems with as many as 1024 channels are coming into use.

The offset dimension adds three important aspects to reflection seismology. First, it enables us to routinely measure the velocity of seismic waves in rocks. This velocity has been assumed to be known in the previous chapters of this book. Second, it gives us data redundancy: it gives independent measurements of quantities that should be the same. Superposition of the measurements (stacking) offers the potential for signal enhancement by destructive interference of noise. Third (a disadvantage), since the offset is nonzero, procedures for migration take on another element of complexity. By the end of this chapter we will be trying to deal with three confusing subjects at the same time—dip, offset, and lateral velocity variation.

Theoretically it seems that offset should offer us the possibility of identifying rocks by observing the reflection coefficient as a function of angle, both for P waves and for P-to-S converted waves. The reality seems to be that neither measurement can be made reliably, if at all. See elswhere in this book a fuller discussion of converted waves, an interesting subject for research, with a large potential for practical rewards. See also Ostrander [1984] and Tatham and Stoffa [1976]. The reasons for the difficulty in measurement, and the resolution of the difficulty, are, however, not the goal of this book. This goal is instead to enable us to deal effectively with that which is routinely observable.

6.0.6 Stacking diagrams

First, define the midpoint y between the shot and geophone, and define h to be half the horizontal offset between the shot and geophone:

$$y = \frac{g + s}{2} \tag{6.1}$$

$$h = \frac{g - s}{2} \tag{6.2}$$

The reason for using *half* the offset in the equations is to simplify and symmetrize many later equations. Offset is defined with $g - s$ rather than with $s - g$ so that positive offset means waves moving in the positive x direction. In the marine case, this means the ship is presumed to sail negatively along the x-axis. In reality the ship may go either way, and shot points may either increase or decrease as the survey proceeds. In some situations you can clarify matters by setting the field observer's shot-point numbers to negative values.

Data is defined experimentally in the space of $(s,\ g)$. Equations (6.1) and (6.2) represent a change of coordinates to the space of $(y,\ h)$. Midpoint-offset coordinates are especially useful for interpretation and data processing. Since the data is also a function of the travel time t, the full dataset lies in a volume. Because it is so difficult to make a satisfactory display of such a volume, what is customarily done is to display slices. The names of slices vary slightly from one company to the next. The following names seem to be well known and clearly understood:

$(y,\ h = 0,\ t)$	zero-offset section
$(y,\ h = h_{\min},\ t)$	near-trace section
$(y,\ h = \text{const},\ t)$	constant-offset section
$(y,\ h = h_{\max},\ t)$	far-trace section
$(y = \text{const},\ h,\ t)$	common-midpoint gather
$(s = \text{const},\ g,\ t)$	field profile (or common-shot gather)
$(s,\ g = \text{const},\ t)$	common-geophone gather
$(s,\ g,\ t = \text{const})$	time slice
$(h,\ y,\ t = \text{const})$	time slice

A diagram of slice names is in Figure 6.1. Figure 6.2 shows three slices from the data volume. The first mode of display is "engineering drawing mode." The second mode of display is on the faces of a cube. But notice that although the data is displayed on the surface of a cube, the slices themselves are taken from the interior of the cube. The intersections of slices across one another are shown by dark lines.

A common-depth-point (CDP) gather is defined by the industry and by common usage to be the same thing as a common-midpoint (CMP) gather. But in this book a distinction will be made. A CDP gather is a CMP gather with its time axis stretched according to some velocity model, say,

$$(y = \text{const},\ h,\ \sqrt{t^2 - 4h^2/v^2} \quad \text{common-depth-point gather}$$

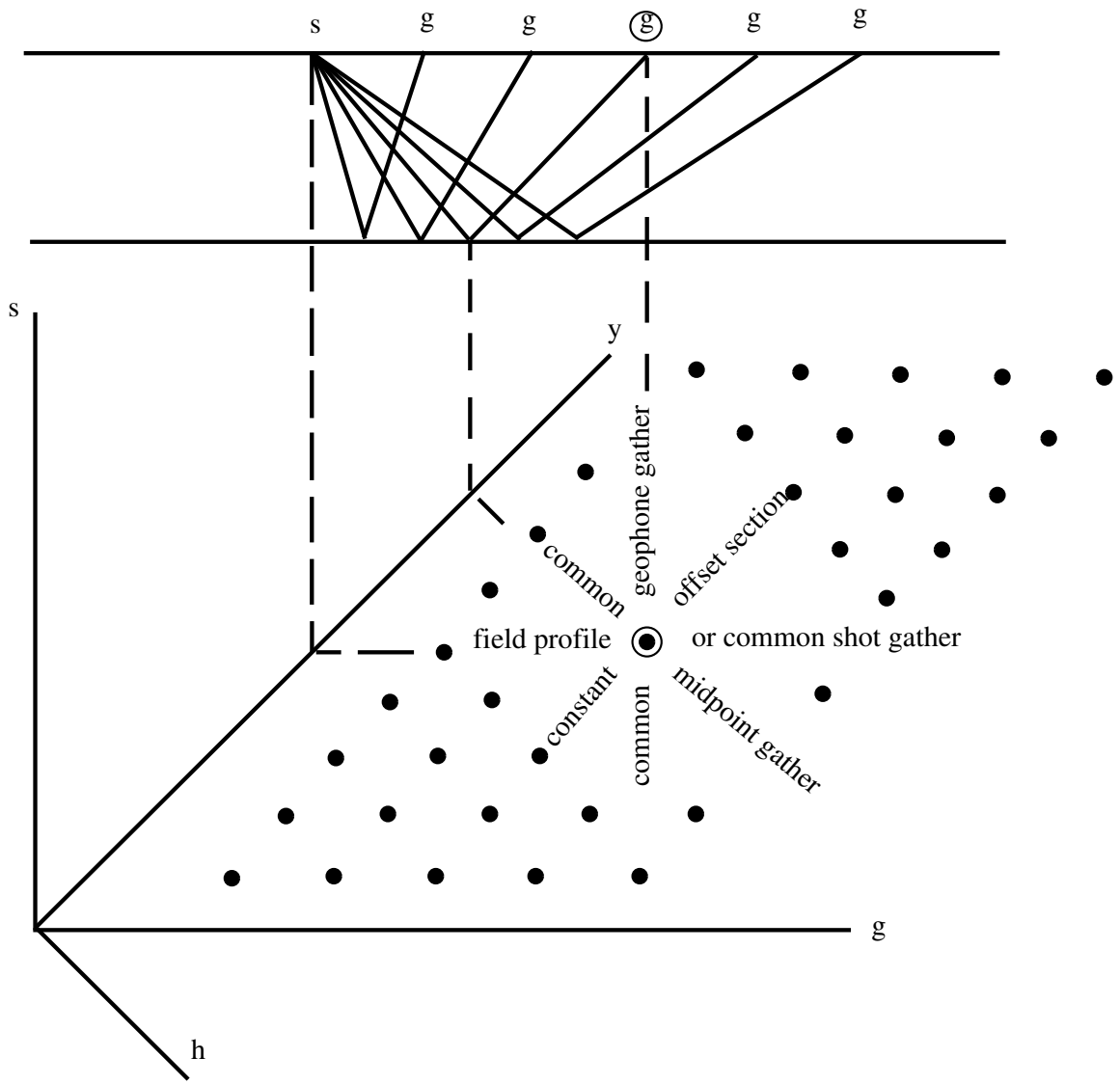

Figure 6.1: Top shows field recording of marine seismograms from a shot at location s to geophones at locations labeled g. There is a horizontal reflecting layer to aid interpretation. The lower diagram is called a stacking diagram. (It is *not* a perspective drawing). Each dot in this plane depicts a possible seismogram. Think of time running out from the plane. The center geophone above (circled) records the seismogram (circled) that may be found in various geophysical displays. Labels in the diagram below give common names for the displays. ofs-sg [NR]

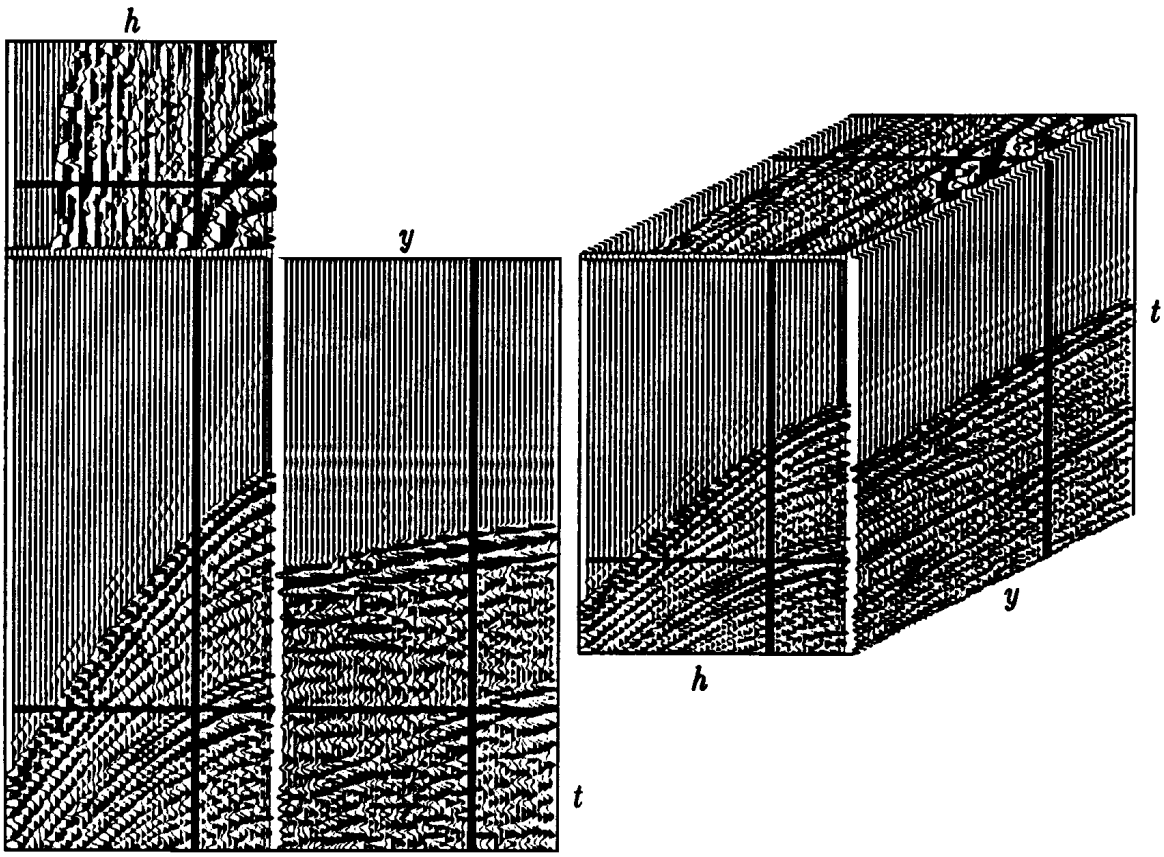

Figure 6.2: Slices from a cube of data from the Grand Banks. Left is "engineering drawing" mode. At the right slices from within the cube are shown as faces on the cube. (Data from Amoco. Display via Rick Ottolini's movie program). ofs-rick [NR]

This offset-dependent stretching makes the time axis of the gather become more like a *depth* axis, thus providing the D in CDP. The stretching is called *normal moveout correction* (NMO). Notice that as the velocity goes to infinity, the amount of stretching goes to zero.

In industrial practice the data is not routinely displayed as a function of offset. Instead, each CDP gather is summed over offset. The resulting sum is a single trace. Such a trace can be constructed at each midpoint. The collection of such traces, a function of midpoint and time, is called a CDP stack. Roughly speaking, a CDP stack is like a zero-offset section, but it has a less noisy appearance.

The construction of a CDP stack requires that a numerical choice be made for the moveout-correction velocity. This choice is called the *stacking velocity*. The stacking velocity may be simply someone's guess of the earth's velocity. Or the guess may be improved by stacking with some trial velocities to see which gives the strongest and least noisy CDP stack.

Figure 6.3 shows typical land and marine profiles (common-shot gathers). The

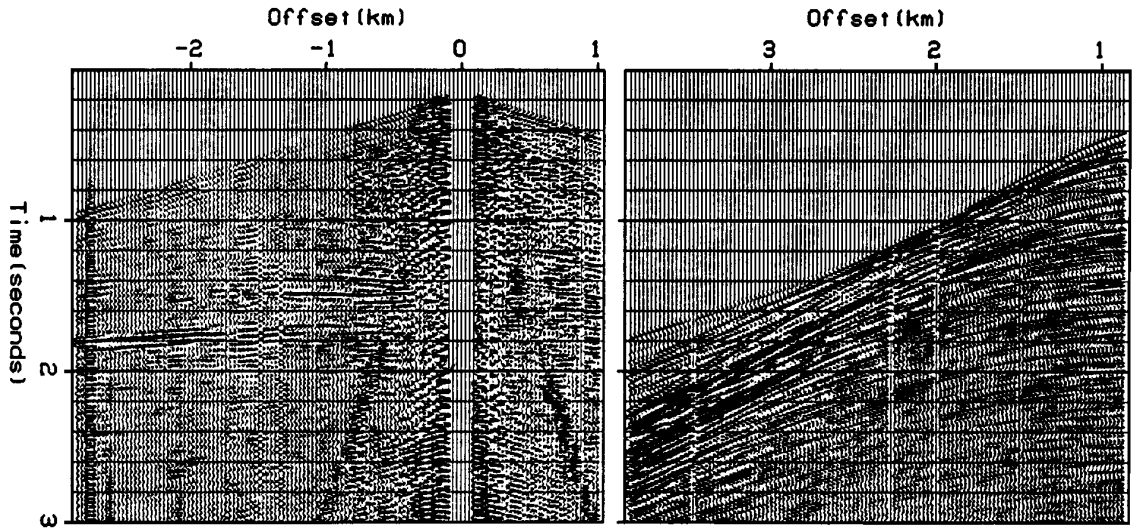

Figure 6.3: Field profiles. Left is a land profile from West Texas. Right is a marine profile off the Aleutian Islands. (Western Geophysical). ofs-profiles [NR]

land data has geophones on both sides of the source. The arrangement shown is called an *uneven split spread*. The energy source was a vibrator. The marine data happens to nicely illustrate two or three head waves. The marine energy source was an air gun. These field profiles were each recorded with about 120 geophones.

6.0.7 What is "poor quality" data?

Vast regions of the world have good petroleum potential but are hard to explore because of the difficulty of obtaining good quality reflection seismic data. The reasons are often unknown. What is "poor quality" data? From an experimental view, almost

all seismic data is good in the sense that it is repeatable. The real problem is that the data makes no sense.

Take as an earth model a random arrangement of point reflectors. Its migrated zero-offset section should look random too. Given the repeatability that is experienced in data collection, data with a random appearance implies a random jumble of reflectors. With only zero-offset data little else can be deduced. But with the full range of offsets at our disposal, a more thoughtful analysis can be tried. This chapter provides some of the required techniques.

An interesting model of the earth is a random jumble of point scatterers in a constant-velocity medium. The data would be a random function of time and a random function of the horizontal location of the shot-geophone midpoint. But after suitable processing, for each midpoint, the data should be a perfectly hyperbolic function of shot-geophone offset. This would determine the earth velocity exactly, even if the random scatterers were distributed in three dimensions, and the survey were only along a surface line.

This particular model could fail to explain the "poor quality" data. In that case other models could be tried. The effects of random velocity variations in the near surface or the effects of multiple reflections could be analyzed. Noise in seismology can usually be regarded as a failure of analysis rather than as something polluting the data. It is the offset dimension that gives us the redundancy we need to try to figure out what is really happening.

6.0.8 Texture of horizontal bedding, marine data

Gravity is a strong force for the stratification of rocks, and in many places in the world rocks are laid down in horizontal beds. Yet even in the most ideal environment the bedding is not mirror smooth; it has some *texture.* We begin the study of offset with synthetic data that mimics the most ideal environment. Such an environment is almost certainly marine, where sedimentary deposition can be slow and uniform. The wave velocity will be taken to be constant, and all rays will reflect as from horizontally lying mirrors. Mathematically, *texture* is introduced by allowing the reflection coefficients of the beds to be laterally variable. The lateral variation is presumed to be a random function, though not necessarily with a white spectrum. Let us examine the appearance of the resulting field data.

Randomness is introduced into the earth with a random function of midpoint y and depth z. This randomness is impressed on some geological "layer cake" function of depth z. For every point in (y, z)-space, a hyperbola of the appropriate random amplitude must be superposed in the space of offset h and travel time t.

What does the final data space look like? This question has little meaning until we decide how the three-dimensional data volume will be presented to the eye. Let us view the data much as it is recorded in the field. For each shot point we see a frame in which the vertical axis is the travel time and the horizontal axis is the distance from

the ship down the towed hydrophone cable. The next shot point gives us another frame. Repetition gives us the accompanying program that produces a cube of data, hence a move. This cube is synthetic data for the ideal marine environment. And what does the movie show?

```
subroutine synmarine ( data, nt,nh,ny, nz)
integer                      nt,nh,ny, nz,    it,ih,iy,is,iz, ns, iseed
          real          data( nt,nh,ny),       layer, rand01
temporary real                              refl(nz,ny), depth(nz)
iseed= 1992;    ns = ny
do iz= 1, nz {                                      # 0 < rand01() < 1
        depth( iz) =  nt * rand01(iseed)            # Reflector depth
        layer      =  2. * rand01(iseed) - 1.       # Reflector strength
        do iy= 1, ny {                              # Impose texture on layer
                refl(iz,iy) = layer * (1. + rand01(iseed))
                }
        }
call null(              data, nt*nh*ny)             # erase data space
do is= 1, ns    {                                   # shots
do ih= 1, nh    {                                   # down cable h = (g-s)/2
do iz= 1, nz    {                                   # Add hyperbola for each layer
        iy = (ns-is)+(ih-1)                         # y = midpoint
        iy = 1 + (iy-ny*(iy/ny))                    # periodic with midpoint
        it = 1 + sqrt( depth(iz)**2 + 25.*(ih-1)**2 )
        if( it <= nt)
                data(it,ih,is) = data(it,ih,is) + refl(iz,iy)
        }}}
return; end
```

A single frame shows hyperbolas with imposed texture. The movie shows the texture moving along each hyperbola to increasing offsets. (I find that no sequence of still pictures can give the impression that the movie gives). Really the ship is moving; the texture of the earth is remaining stationary under it. This is truly what most marine data looks like, and the subroutine `synmarine()` simulates it.

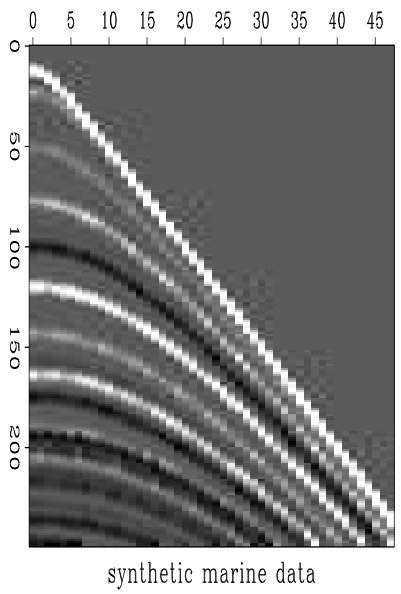

Figure 6.4: A frame from the synthetic marine data subroutine `synmarine()`. Press button for movie. ofs-synmarine [ER]

Comparing the simulated data to real marine-data movies, I am impressed by the large amount of random lateral variation required in the simulated data to achieve resemblance to field data. The randomness seems too great to represent lithologic variation. Apparently it is the result of something not modeled. Perhaps it results from our incomplete understanding of the mechanism of reflection from the quasi-random earth. Or perhaps it is an effect of the partial focusing of waves sometime after they reflect from minor topographic irregularities.

6.0.9 Texture of land data: near-surface problems

Reflection seismic data recorded on land frequently displays randomness because of the irregularity of the soil layer. Often it is so disruptive that the seismic energy sources are deeply buried (at much cost). The geophones are too many for burial. For most land reflection data, the texture caused by these near-surface irregularities exceeds the texture resulting from the reflecting layers.

To clarify our thinking, an ideal mathematical model will be proposed. Let the reflecting layers be flat with no texture. Let the geophones suffer random time delays of several time points. Time delays of this type are called *statics.* Let the shots have random strengths. For this movie, let the data frames be *common-midpoint gathers,* that is, let each frame show data in (h, t)-space at a fixed midpoint y. Successive frames will show successive midpoints. The study of Figure 6.1 should convince you that the travel-time irregularities associated with the geophones should move leftward, while the amplitude irregularities associated with the shots should move rightward. In real life, both amplitude and time anomalies are associated with both shots and geophones.

EXERCISES:

1 Note that Figure 6.1 is drawn for a shot interval Δs equal to half the geophone interval Δg. Redraw Figure 6.1 for $\Delta s = \Delta g$. Common-midpoint gathers now come in two types. Suggest two possible definitions for "near-offset section."

2 Modify the program of Figure 6.5 to produce a movie of synthetic *midpoint* gathers with random shot amplitudes and random geophone time delays. Observing this movie you will note the perceptual problem of being able to see the leftward

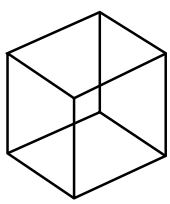

Figure 6.5: ofs-cube [NR]

motion along with the rightward motion. Try to adjust anomaly strengths so that both left-moving and right-moving patterns are visible. Your mind will often see only one, blocking out the other, similar to the way you perceive a 3-D cube, from a 2-D projection of its edges.

3 Define recursive dip filters to pass and reject the various textures of shot, geophone, and midpoint.

6.1 ABSORPTION AND A LITTLE FOCUSING

Sometimes the earth strata lie horizontally with little irregularity. There we may hope to ignore the effects of migration. Seismic rays should fit a simple model with large reflection angles occurring at wide offsets. Such data should be ideal for the measurement of reflection coefficient as a function of angle, or for the measurement of the earth acoustic absorptivity $1/Q$. In his doctoral dissertation, Einar Kjartansson reported such a study. The results were so instructive that the study will be thoroughly reviewed here. I don't know to what extent the Grand Isle gas field (Pan [1983]) typifies the rest of the earth, but it is an excellent place to begin learning about the meaning of shot-geophone offset.

6.1.1 The grand isle gas field: a classic bright spot

The dataset Kjartansson studied was a seismic line across the Grand Isle gas field, off the shore of Louisiana, and was supplied by the Gulf Oil Company. The data contain several classic "bright spots" (strong reflections) on some rather flat undisturbed bedding. Of interest are the lateral variations in amplitude on reflections at a time depth of about 2.3 seconds. (See Figure 6.8. It is widely believed that such bright spots arise from shallow gas-bearing sands.

Theory predicts that reflection coefficient should be a function of angle. For an anomalous physical situation like gas-saturated sands, the function should be distinctive. Evidence should be found on common-midpoint gathers like those shown in Figure 6.6. Looking at any one of these gathers you will note that the reflection strength versus offset seems to be a smooth, sensibly behaved function, apparently quite measurable. Using layered media theory, however, it was determined that only the most improbably bizarre medium could exhibit such strong variation of reflection coefficient with angle, particularly at small angles of incidence. (The reflection angle of the energy arriving at wide offset at time 2.5 seconds is not a large angle. Assuming constant velocity, $\arccos(2.3/2.6) = 28^\circ$). Compounding the puzzle, each common-midpoint gather shows a *different* smooth, sensibly behaved, measurable function. Furthermore, these midpoints are near one another, ten shot points spanning a horizontal distance of 820 feet.

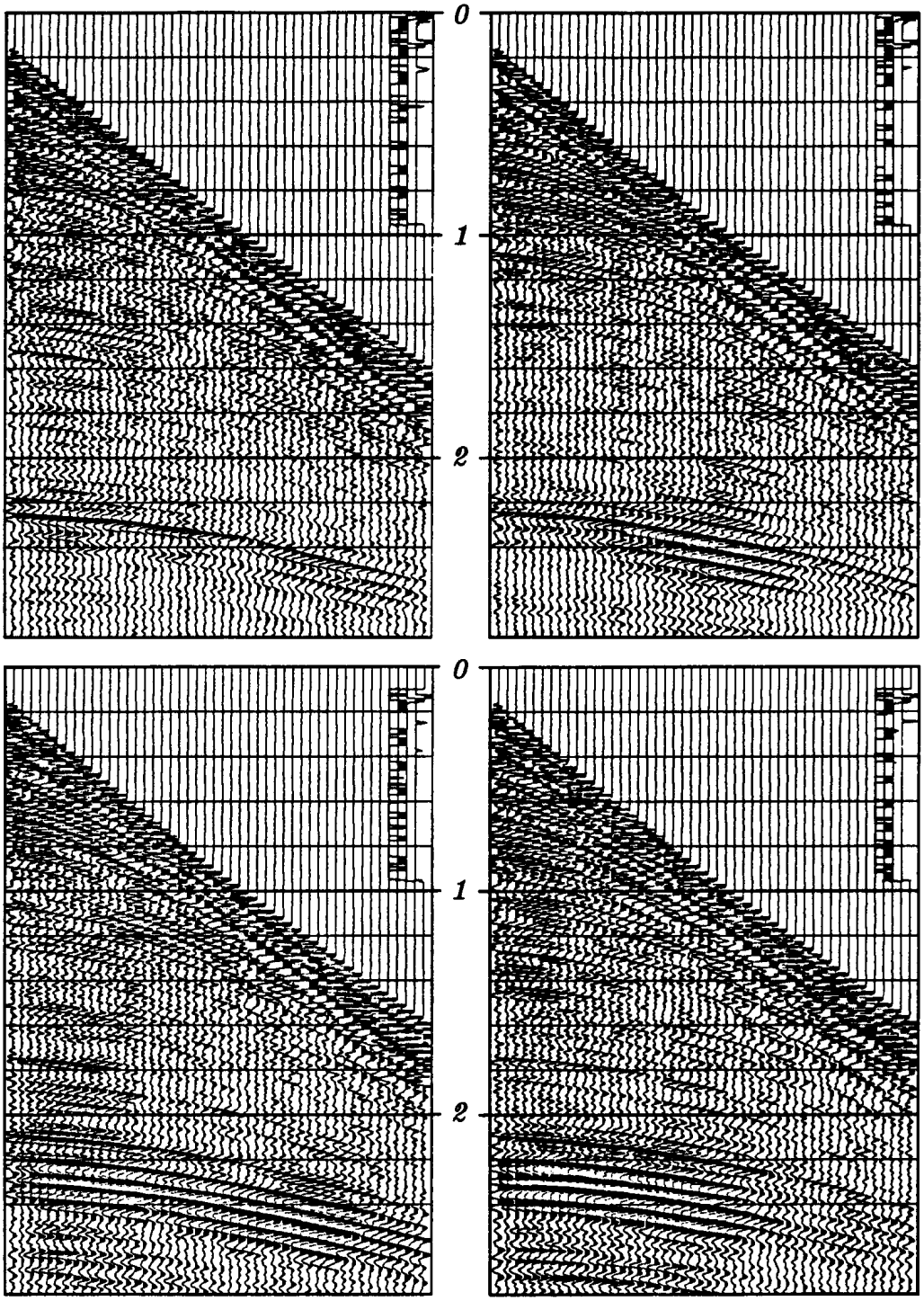

Figure 6.6: Top left is shot point 210; top right is shot point 220. No processing has been applied to the data except for a display gain proportional to time. Bottom shows shot points 305 and 315. (Kjartansson, Gulf) ofs-kjcmg [NR]

6.1.2 Kjartansson's model for lateral variation in amplitude

The Grand Isle data is incomprehensible in terms of the model based on layered media theory. Kjartansson proposed an alternative model. Figure 6.7 illustrates a geometry in which rays travel in straight lines from any source to a flat horizontal reflector, and thence to the receivers. The only complications are "pods" of some material

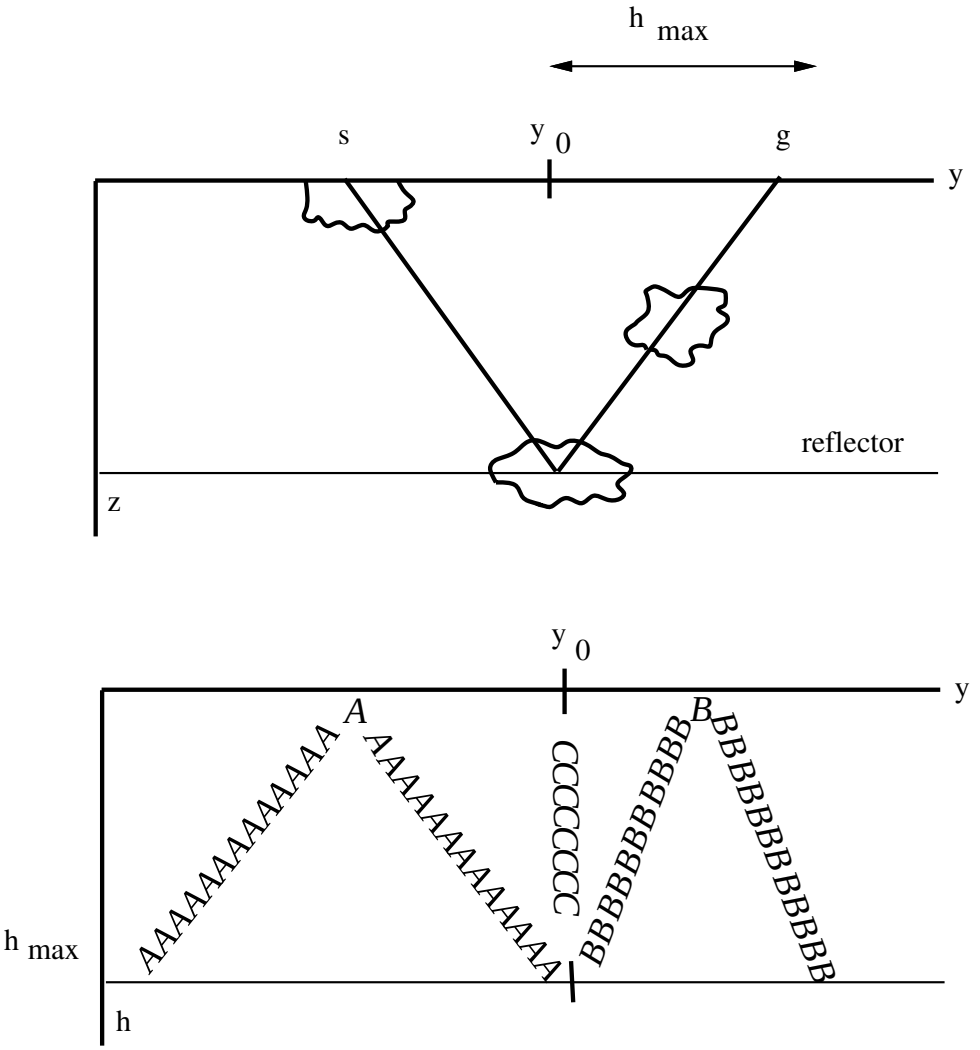

Figure 6.7: Kjartansson's model. The model on the top produces the disturbed data space sketched below it. Anomalous material in pods A, B, and C may be detected by its effect on reflections from a deeper layer. ofs-kjidea [NR]

that is presumed to disturb seismic rays in some anomalous way. Initially you may imagine that the pods absorb wave energy. (In the end it will be unclear whether the disturbance results from energy focusing or absorbing).

Pod A is near the surface. The seismic survey is affected by it twice—once when the pod is traversed by the shot and once when it is traversed by the geophone. Pod C is near the reflector and encompasses a small area of it. Pod C is seen at all offsets

h but only at one midpoint, y_0. The raypath depicted on the top of Figure 6.7 is one that is affected by all pods. It is at midpoint y_0 and at the widest offset $h_{\max}$. Find the raypath on the lower diagram in Figure 6.7.

Pod B is part way between A and C. The slope of affected points in the (y, h)-plane is part way between the slope of A and the slope of C.

Figure 6.8 shows a common-offset section across the gas field. The offset shown is the fifth trace from the near offset, 1070 feet from the shot point. Don't be tricked into thinking the water was deep. The first break at about .33 seconds is wide-angle propagation.

The power in each seismogram was computed in the interval from 1.5 to 3 seconds. The logarithm of the power is plotted in Figure 6.9a as a function of midpoint and offset. Notice streaks of energy slicing across the (y, h)-plane at about a 45° angle. The strongest streak crosses at exactly 45° through the near offset at shot point 170. This is a missing shot, as is clearly visible in Figure 6.8. Next, think about the gas sand described as pod C in the model. Any gas-sand effect in the data should show up as a streak across all offsets at the midpoint of the gas sand—that is, horizontally across the page. I don't see such streaks in Figure 6.9a. Careful study of the figure shows that the rest of the many clearly visible streaks cut the plane at an angle noticeably *less* than $\pm 45°$. The explanation for the angle of the streaks in the figure is that they are like pod B. They are part way between the surface and the reflector. The angle determines the depth. Being closer to 45° than to 0°, the pods are closer to the surface than to the reflector.

Figure 6.9b shows timing information in the same form that Figure 6.9a shows amplitude. A CDP stack was computed, and each field seismogram was compared to it. A residual time shift for each trace was determined and plotted in Figure 6.9b. The timing residuals on one of the common-midpoint gathers is shown in Figure 6.10.

The results resemble the amplitudes, except that the results become noisy when the amplitude is low or where a "leg jump" has confounded the measurement. Figure 6.9b clearly shows that the disturbing influence on timing occurs at the same depth as that which disturbs amplitudes.

The process of *inverse slant stack*, to be described in Section 5.2 enables us to determine the depth distribution of the pods. This distribution is displayed in figures 6.9c and 6.9d.

6.1.3 Rotten alligators

The sediments carried by the Mississippi River are dropped at the delta. There are sand bars, point bars, old river bows now silted in, a crow's foot of sandy distributary channels, and between channels, swampy flood plains are filled with decaying organic material. The landscape is clearly laterally variable, and eventually it will all sink of its own weight, aided by growth faults and the weight of later sedimentation. After

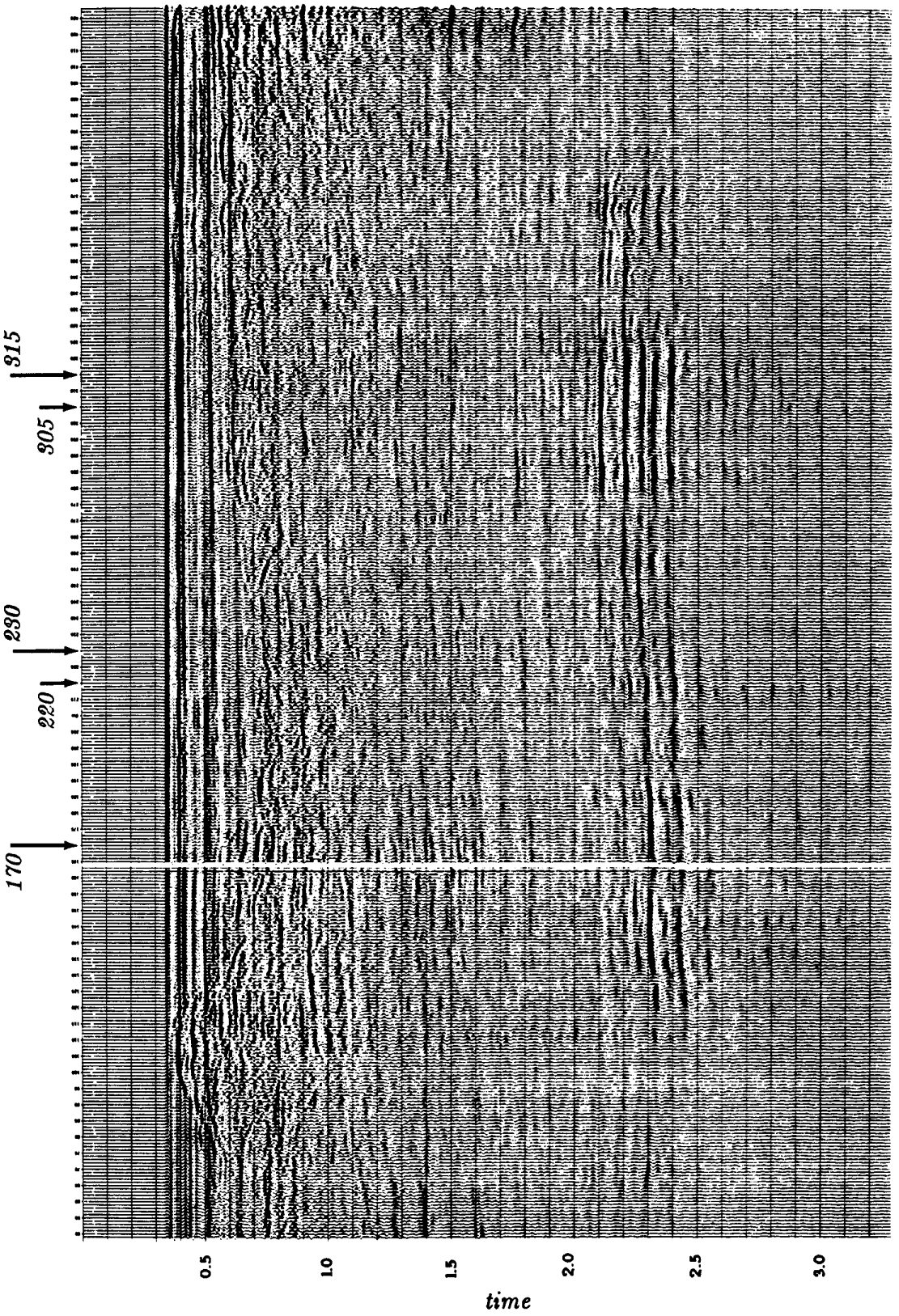

Figure 6.8: A constant-offset section across the Grand Isle gas field. The offset shown is the fifth from the near trace. (Kjartansson, Gulf) ofs-kjcos [NR]

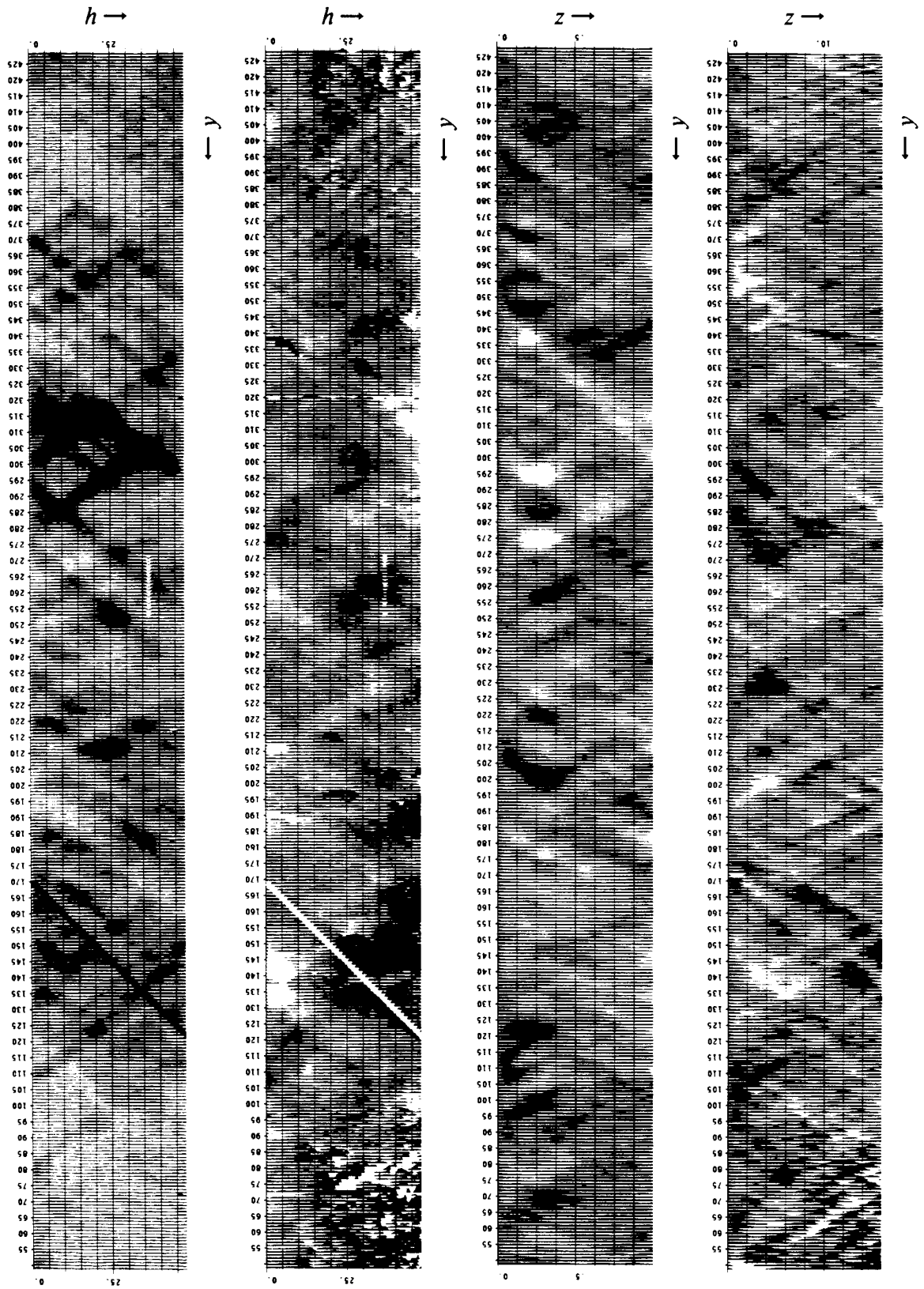

Figure 6.9: (a) amplitude (h,y), (b) timing (h,y) (c) amplitude (z,y), (d) timing (d,y) ofs-kja [NR]

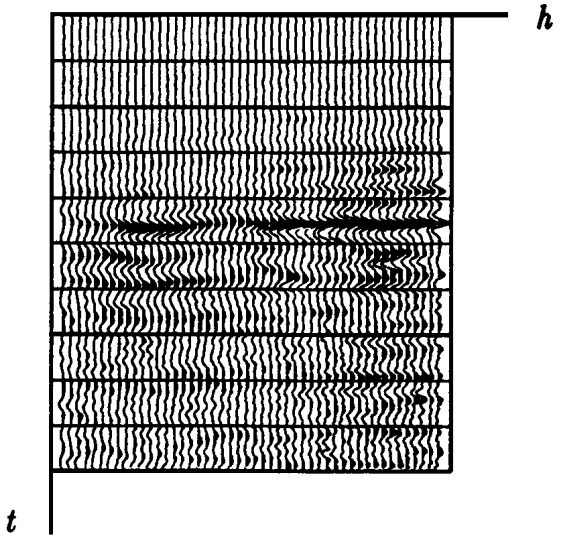

Figure 6.10: Midpoint gather 220 (same as timing of (h,y) in Figure 6.9b) after moveout. Shown is a one-second window centered at 2.3 seconds, time shifted according to an NMO for an event at 2.3 seconds, using a velocity of 7000 feet/sec. (Kjartansson) ofs-kjmid [NR]

it is buried and out of sight the lateral variations will remain as pods that will be observable by the seismologists of the future. These seismologists may see something like Figure 6.11. Figure 6.11 shows a *three-dimensional* seismic survey, that is, the ship sails many parallel lines about 70 meters apart. The top plane, a slice at constant time, shows buried river meanders. The data shown in Figure 6.11 is described more fully by its donors, Dahm and Graebner [1982].

6.1.4 Focusing or absorption?

Highly absorptive rocks usually have low velocity. Behind a low velocity pod, waves should be weakened by absorption. They should also be strengthened by focusing. Which effect dominates? How does the phenomenon depend on spatial wavelength? A full reconstruction of the physical model remains to be done. Maybe you can figure it out knowing that black on Figure 6.9c denotes low amplitude or high absorption, and black on Figure 6.9d denotes low velocities.

EXERCISES:

1 Consider waves converted from pressure P waves to shear S waves. Assume an S-wave speed of about half the P-wave speed. What would Figure 6.7 look like for these waves?

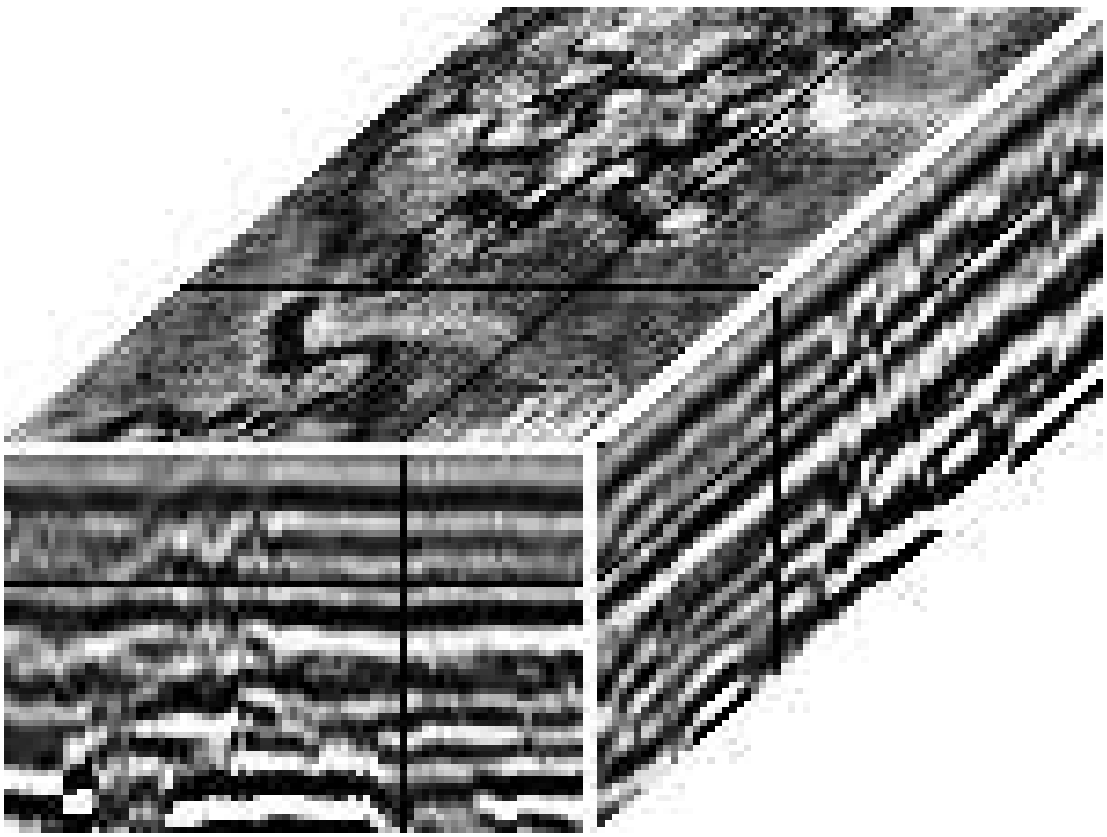

Figure 6.11: Three-dimensional seismic data (Geophysical Services Inc.) from the Gulf of Thailand. Data planes from within the cube are displayed on the faces of the cube. The top plane shows ancient river meanders now submerged. ofs-meander [ER]